A Reggeized model for η meson production in high energy proton/proton collisions.

A Thesis
Presented to
The Division of Mathematics and Natural Sciences
Reed College

In Partial Fulfillment
of the Requirements for the Degree
Bachelor of Arts

Adarsh Pyarelal

May 2011

Approved for the Division
(Physics)

_____

Nelia Mann

Preface

At the beginning of the year, it was with barely contained enthusiasm that I told everyone who cared to ask that my thesis was related to string theory. Indeed, this notion provided much of my momentum last fall. Now, at the other end of the tunnel, with a thesis only tangentially related to string theory, I am still fascinated by elementary particle physics - it is a vast, often messy topic, but the hints of an elegant framework underlying the fundamental constituents of matter and their interactions make it a subject well worth pursuing.

As I write this, I am preparing to go to the University of Arizona to begin graduate work in physics this fall, and will likely continue studying particle physics. The Large Hadron Collider has started running again after a few initial setbacks, and the mood among particle physicists is one of elation. As experimentalists navigate the realms of energy made newly accessible by the LHC, some theories will be validated and others cast aside. One thing is for certain - the landscape of particle physics will be irreversibly changed. If we have not verified the standard model of particle physics or discovered new physics beyond it by the time the LHC reaches its maximum capacity, it might be a while before we get a chance to do so again. Particle colliders are becoming prohibitively expensive as they become larger and more powerful, and funding has always been tight, especially since elementary particle physics as a field does not have any obvious applications to industry or national defense. An alternative, less expensive method for investigating elementary particle dynamics may be devised someday, but until then, colliders are our main window into the world of elementary particles.

My thesis is firmly based in this regime. The choice of the neutral pion and the eta (η) meson was in no small part due to the fact that the calculations involving them are relatively tractable and appropriate for an undergraduate senior thesis. My hope is that this thesis can serve as a starting point for theorists interested in modeling high energy hadron scattering.

Adarsh Pyarelal
May 2011
Portland, Oregon, USA

Acknowledgements

I would like to thank my advisor, Nelia Mann, for her guidance over the course of a year and for letting me get a taste of theoretical particle physics research. Her patience and flexibility in response to my frequent scatterbrained-ness went a long way towards making the thesis process much more enjoyable and much less stressful than it could have been (I still learned a few things, I promise!). I would also like to thank the following.

1. Joel Franklin, for letting me do thesis work on Scientific Computation time and for introducing me to the numerical method used for the simulation.
2. Mary Miller, Rao Potluri, and Johnny Powell for a lively discussion at my thesis oral defense.
3. Mary James, Lucas Illing, Nick Wheeler, Darrell Schroeter, David Griffiths and David Latimer, most of whom I have taken classes with, and all of whom I have received sound advice from.
4. Molly King, for her steady love and support these three years, and for making sure that I took care of myself my senior year.
5. Javed Parkes, Kundai Gumbo, Michael Reisor, Advait Jukar, Kyle Lu, and Carolyn Kim for being my best friends in my time at Reed.
6. My fellow denizens of the physics sub-basement, including Teddy, Wally, Colin, Bela, Manu, Todd, Dylan, Max, Moriah, May Ling, Aaron, Jeremy, Mackenzie, Allison, Greg Eibel, and Bob Ormond, for their solidarity and for many great conversations, pub nights, and softball practices.
7. Rabeca, Marianne, Josh, Hollie, Shannon, and Wiley for good times at the computer store and keeping me employed senior year.
8. My host parents, Phil and Dianne Levinson, for providing a home away from home.
9. Reed, for letting me in with nearly a full ride. I am truly grateful for this opportunity.

Last but not least, my family, and especially my parents, V.B. Pyarelal and Suchitra Pyarelal, for believing in me when no one else would. I would not be here if they had not supported me in my (in retrospect) somewhat impetuous decision to invest all my energy in applying to American colleges.

This thesis is dedicated to them.

Table of Contents

Abstract

We develop a model for central production of η mesons in high energy, small angle deflection proton/proton collisions. We calculate the scattering amplitude of the process by substituting a Reggeized neutral pion propagator in place of a spin-0 propagator in the Feynman amplitude. In addition, we implement a rudimentary event generator in *Mathematica* to simulate scattering events according to the calculated differential cross-section. The simulated distribution of events is qualitatively consistent with our model.

Introduction

The standard model of particle physics has stood its ground as the dominant paradigm describing elementary particles and their interactions for over three decades. It postulates that there are three kinds of elementary particles that make up the entire universe: quarks, leptons, and gauge bosons. All the matter that we see around us is made of quarks and leptons. An atom consists of a nucleus of protons and neutrons (collectively known as nucleons) surrounded by a cloud of electrons. Electrons belong to the lepton family, and the nucleons themselves have substructure - they are comprised of quarks. In addition to the nucleons, there are many other possible combinations of quarks that we do not see in everyday life. However, we can observe them through cosmic rays, particle accelerators, and nuclear decays. The gauge bosons are the 'mediators' of the fundamental forces. When we say that a force is mediated by a particular gauge boson, we mean that two particles interacting via that force do so by exchanging that particular gauge boson.[1] The gauge bosons and the interactions they mediate are listed below.

1. The photon is the mediator of the electromagnetic force between electrically charged particles, the force that is responsible for the vast majority of everyday phenomena that we see around us.

2. The W and Z bosons mediate the weak force between particles that carry 'weak charge', a group that includes all quarks and leptons. The weak force is responsible for many radioactive decays.

3. Gluons are the mediators of the strong force between quarks. This is the force that directly binds three quarks into protons or neutrons and two quarks into mesons. The relatively long range residual effect of this force is what is known as the nuclear force, which binds protons and neutrons together in atomic nuclei.

The interactions between protons in this thesis occur via the nuclear force, as we shall see.

[1] Classically, we assume that forces are caused by the influence of a field. For example, a moving electron produces electric and magnetic fields around it. When another charged particle is placed within these fields, it experiences the electromagnetic force. In quantum field theory, these fields are no longer continuous, but discretized. In quantum electrodynamics (QED), photons are the discrete, or *quantized* components of electromagnetic fields.

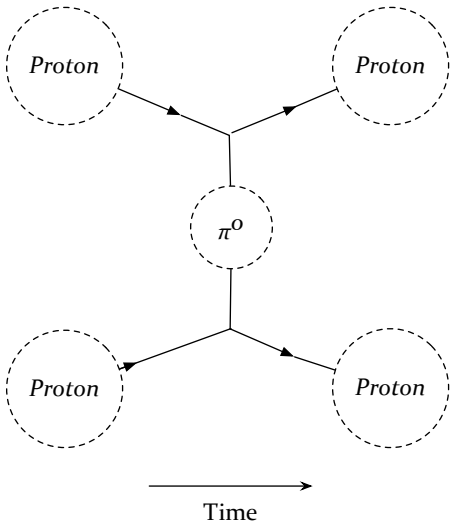

Figure 0.1: A diagram depicting the interaction of two protons via the exchange of a neutral, spin-0 pion. The way to read the diagram is to move your eyes across the page in the direction of the arrow of time. Two protons come together, exchange a pion, and emerge again on the other side. The diagram does not represent any spatial characteristics of the particles - although the protons appear to be diverging, the interaction between them is in fact *attractive*.

The strong force

Long before the establishment of quantum chromodynamics (QCD) as the theory of the strong interaction, Hideki Yukawa proposed in 1934 that the force that holds the nuclei of atoms together arises from the exchange of pi-mesons, or 'pions', as shown in Figure 0.1. The existence of these particles was confirmed in 1947 [7]. However, this is a simplified picture of the actual process, depicted in Figure 0.2. As you can see, the mechanism is much more complicated, involving the quarks that comprise the protons and the pion, and the gluons that mediate the strong interactions between the quarks. However, free quarks are never observed in nature - they occur only in bound doublet or triplet states. This phenomenon is known as 'quark confinement'. These bound states interact via the residual 'nuclear force' which has a very short range, and can be modeled using the exchange of mesons. This model is effective and accurate enough for us to keep using, especially since realistic QCD models for this type of interaction are usually prohibitively complicated and require immense amounts of computing power to simulate.

Regge trajectories

In many families of hadrons[2] whose members differ only in their masses and spins, there is a linear relationship between the spins and the squares of the masses of some of these members. The emergence of this pattern in the ρ and the a meson families are shown in Figure Figure 0.3. The members of these families are plotted on a *Chew-Frautschi* plot in which the horizontal axis represents the square of the masses of the particles, and the vertical axis their spin. The linear function that fits this pattern is known as the *Regge trajectory*. The mathematical framework that shows that particles with differ-

[2]This term refers to the two kinds of particles that are made of quarks - baryons such as the protons and neutrons, and mesons such as the pion.

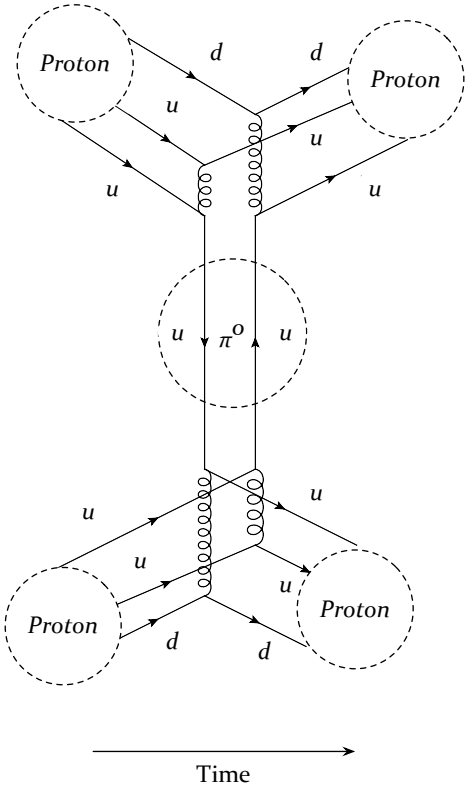

Figure 0.2: The mechanism of proton-proton interaction through pion exchange as interpreted in QCD. The lines labeled u and d represent two of the six 'flavors' of quark. In this model each proton consists of two 'up' quarks and one 'down' quark, and the neutral spin-0 pion consists of an up quark and its antiparticle. The spiral lines connecting the quarks represent gluons mediating the strong interaction.

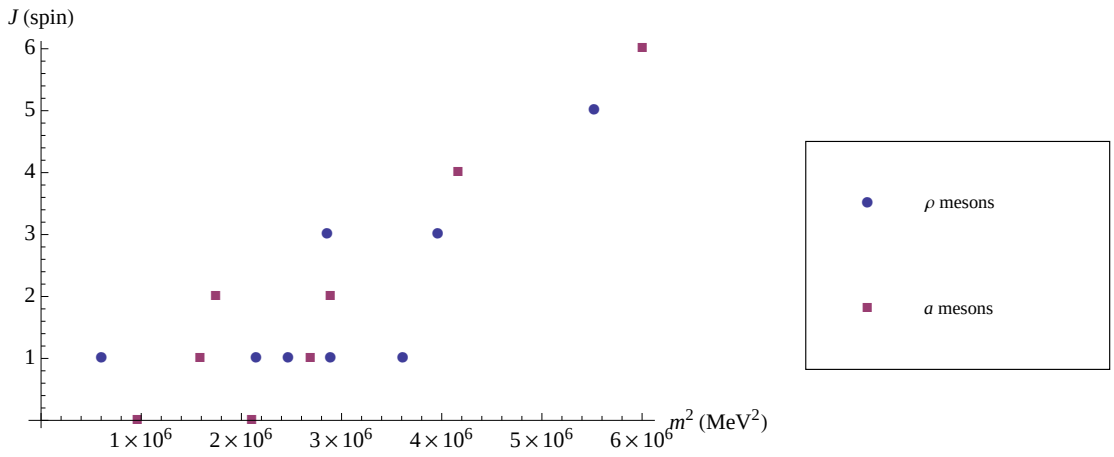

Figure 0.3: Regge trajectories for the ρ and a families of mesons. As you can see, there are separate families of mesons (even spin ρ and odd spin a mesons) that lie on the same Regge trajectory. The unit of mass here is MeV, or mega electron volts (usually a unit of energy, but we will be working in Planck units where the units of mass and energy are the same). All particle data in this thesis is from the Particle Data Group at Lawrence Berkeley National Laboratory [10].

ent spins are related by the Regge trajectory function is known as Regge theory[3], formulated by Tullio Regge in 1959 [12]. Out of all the members of a hadron family, the particles that lie upon the Regge trajectory have the greatest effect on scattering events. At low energies, considering the exchange of just the familiar, spin-0 neutral pion would be enough to model scattering via the nuclear interaction. However, at high energies we must include the contribution of the entire family of particles on the neutral pion Regge trajectory. The main objective of this thesis is to develop a model that takes into account all of these contributions. Regge theory leads to the use of a phenomenological expression for 2-2 hadron scattering via the nuclear force known as the Veneziano amplitude, which takes into account the exchange of all the particles that lie on the Regge trajectory.

Connection with string theory

It turns out that the pattern of mesons on the Chew-Frautschi plot arises naturally from string theory - the various members of the meson family correspond to internal excitations of the same type of open string. In addition, the Veneziano amplitude corresponds to the amplitude for open-string scattering in string theory.

String theory is notorious for not making sharp, testable predictions - the theory is still not understood well enough [14] and the energies required to directly probe the associated length scale are many orders of magnitude greater than what we can produce right now [5]. However, we can use the Veneziano amplitude to construct models for scattering involving the exchange of Regge trajectories. This provides a use for string theory as a tool for building phenomenological models that can be compared directly to data.

Scattering: a window into the world of elementary particles

Elementary particle scattering corresponds roughly to the image that the phrase generates in the mind's eye: tiny particles are shot at each other at very high speeds and bounce off in different directions (sometimes producing other tiny particles). Indeed, who would have thought that such a seemingly haphazard process would be our primary source of information about the fundamental constituents of matter?

Yet particle colliders are the workhorses of experimental particle physics, consistently producing new data about elementary particles[4]. Well known particle accelerators include the Tevatron at Fermilab, the Relativistic Heavy Ion Collider at Brookhaven, SLAC at Stanford, and of course, the infamous Large Hadron Collider (LHC) at CERN in Geneva. Most of the particle physics discoveries of the next decade are expected to take place at the LHC, including (hopefully) the discovery of the Higgs boson[5] and perhaps even some signs of physics beyond the standard model.

Elementary particles are simply too small to be directly observed, say by putting them under a microscope. We have to resort to other methods, out of which scattering experiments form a large chunk. At high energies, we can 'push' particles closer together to ensure that they interact with each

[3]For a thorough introduction to Regge theory, see [3].

[4]Until, that is, they reach their maximum energy levels, and we scramble to put together funding for an even bigger one!

[5]The Higgs boson is the last remaining brick in the foundation of the standard model, which predicts that matter acquires mass by interacting with the corresponding 'Higgs field'.

other. These interactions are quite complicated, as you have seen in Figure 0.2, and their outcomes can tell us much about the particles involved.

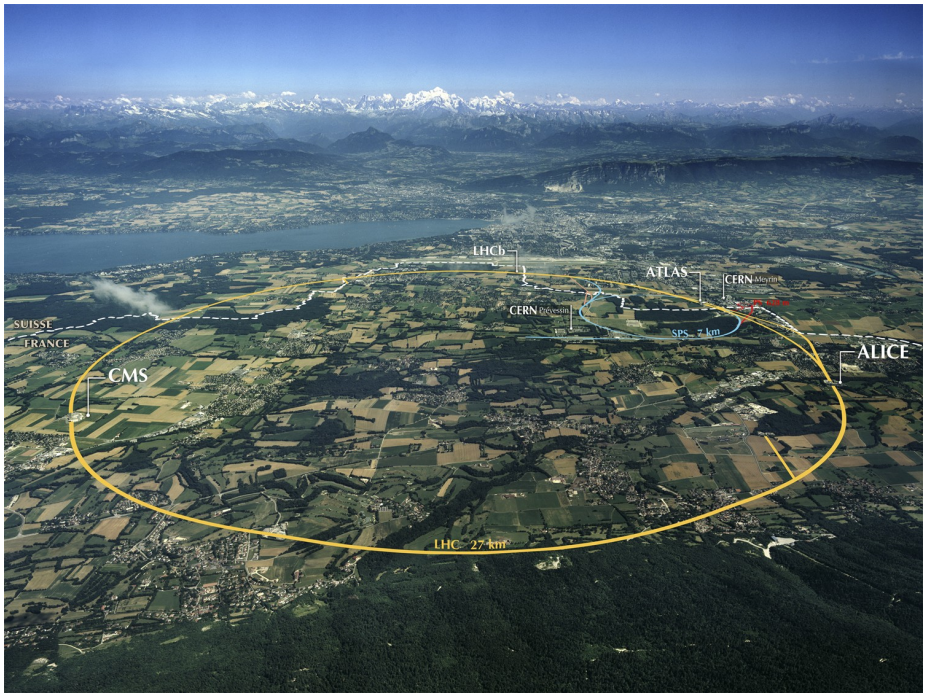

Figure 0.4: Aerial view of the Large Hadron Collider, which is 27 kilometers in diameter. ATLAS, CMS, ALICE and LHCb are the four large experiments situated on the LHC ring. (Courtesy CERN.)

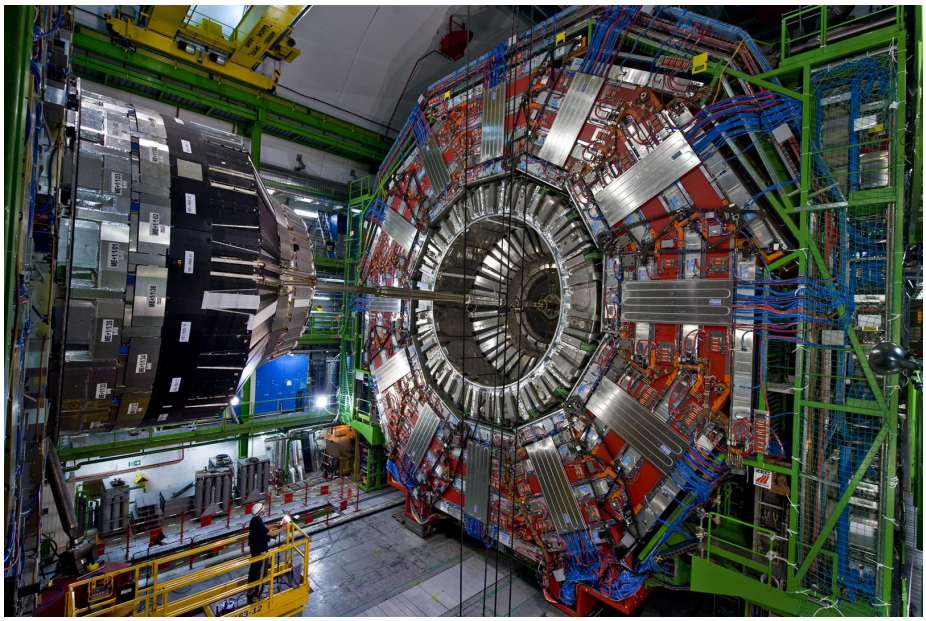

Figure 0.5: The CMS (compact muon solenoid) experiment/particle detector at the LHC. (Courtesy CERN.)

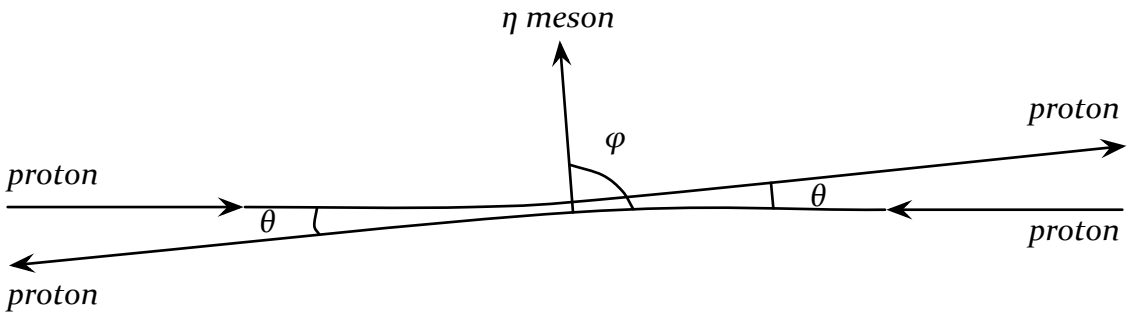

Figure 0.6: Envisioning the scattering event in the frame of reference where the center of mass of the system is at rest. The particles scatter at a small angle θ and produce an extra particle, an η meson.

Central production of η mesons in proton/proton collisions

The reaction that we will attempt to model is $p + p \rightarrow p + p + \eta$. It has been studied extensively, for example by the DISTO collaboration [1]. The mechanism of production of the η meson is still not well known. It is thought to involve the exchange of η, π, ρ and ω mesons, but so far it has not been possible to definitively disentangle these contributions. The model in this thesis could be used to gain some insight into this mechanism. Figure 0.6 shows a simple representation of the scattering process. We will be assuming that the initial protons are fired straight at each other, interact briefly and continue onwards with a slight deflection, producing an η meson in the process.

A roadmap for the thesis

The first thing we will do in this thesis is establish the relativistic kinematics of a single scattering event - we will impose the conservation of energy and momentum and the 'mass shell conditions', and also express all the kinematic parameters involved in terms of 'Mandelstam variables'. In the second chapter, we will introduce scattering theory and how it relates to experiment. We will also set up the problem in terms of the four parameters that are actually measured experimentally. The third chapter is where we will deal with the actual dynamics of the process, that is, the strong force interactions mediated by the exchange of pions. We will use the Veneziano amplitude to sum the contributions of the whole family of pions. In the fourth chapter, we will finally simulate the experiment by numerically generating events, or combinations of particle parameters, according to our model.

Chapter 1

Relativistic Kinematics of 2-3 Scattering

In this chapter we will set up the relativistic kinematics for the 2-3 (two particles in, three particles out) process $p + p \rightarrow p + p + \eta$. This involves imposing kinematical constraints such as the conservation of energy and momentum and the mass shell conditions and performing the approximations required for high energy, small-angle scattering. We will only be dealing with the *kinematics* of the collision here, ignoring the dynamics introduced by quantum mechanical effects and the strong force. All you really need to know here is that two protons are initially fired at each other along the z-axis at very high energies and are deflected by a small angle, and that the final state consists of these two protons and an η meson.

1.1 Notation

The calculations in this chapter can get a bit dense sometimes. Internalizing the notation conventions described below will go a long way in helping understand the rest of the chapter.

1. p_i denotes the energy-momentum 4-vector of the i^{th} particle, with the components $(E_i, p_{ix}, p_{iy}, p_{iz})$.
2. $\mathbf{p}_i$ denotes the spatial momentum 3-vector of the i^{th} particle, with components (p_{ix}, p_{iy}, p_{iz}).
3. $\mathbf{q}_i$ denotes the component of the momentum of the i^{th} particle lying in the plane transverse to the collision, *i.e.* in the $x-y$ plane, with components $(q_{ix}, q_{iy}) = (p_{ix}, p_{iy})$.
4. p^2 represents the invariant product $p_\mu p^\mu$.[1] The Einstein summation convention (summing over repeated indices) is used here.
5. $|\mathbf{p}_i| = \sqrt{p_{ix}^2 + p_{iy}^2 + p_{iz}^2}$ and $\mathbf{p}_i^2 = |\mathbf{p}_i|^2$
6. $q_i = |\mathbf{q}_i| = \sqrt{q_{ix}^2 + q_{iy}^2}$
7. $p_i = (E_i, \mathbf{p}_i) = (E_i, \mathbf{q}_i, p_{iz}) = (E_i, q_{ix}, q_{iy}, p_{iz})$

[1] The invariant product is the product $p^\mu \eta_{\mu\nu} p^\nu$, where $\eta_{\mu\nu}$ is the Minkowski metric, represented by $\begin{pmatrix} 1 & 0 & 0 & 0 \\ 0 & -1 & 0 & 0 \\ 0 & 0 & -1 & 0 \\ 0 & 0 & 0 & -1 \end{pmatrix}$.

8. m_p and m_η are the masses of the proton and the η meson respectively.

We will be working in Planck units, where we set the speed of light to be $c = 1$.

For our process we will label the incoming protons particles 1 and 2, the outgoing protons particles 3 and 4, and the meson particle 5. The 4-momentum vectors of these particles are written below, consistent with our notation scheme.

1. $p_1 = (E_1, p_{1x}, p_{1y}, p_{1z}) = (E, 0, 0, p)$
2. $p_2 = (E_2, p_{2x}, p_{2y}, p_{2z}) = (E, 0, 0, -p)$
3. $p_3 = (E_3, p_{3x}, p_{3y}, p_{3z}) = (E_3, q_{3x}, q_{3y}, p_{3z}) = (E, \mathbf{q}_3, p_{3z})$
4. $p_4 = (E_4, p_{4x}, p_{4y}, p_{4z}) = (E_4, q_{4x}, q_{4y}, p_{4z}) = (E, \mathbf{q}_4, p_{4z})$
5. $p_5 = (E_5, p_{5x}, p_{5y}, p_{5z}) = (E_5, q_{5x}, q_{5y}, p_{5z}) = (E, \mathbf{q}_5, p_{5z})$

The components of p_1 and p_2 are set by the experiment. All quantities are described in the center of momentum (CM) frame where the total spatial momentum of the system is zero.

1.2 Constraining our parameters

With five particles in the process (two incoming, three outgoing) and four parameters that describe each one (the components of its 4-momentum), we have 20 parameters in total that we need to deal with. However, as we shall see, the majority of them are constrained through experimental or kinematical considerations.

Experimental constraints

From the outset, eight of these parameters - the energies and spatial momenta of the two incoming protons - are determined by the design of the experiment. This leaves us with twelve parameters.

Conservation of energy and momentum

From the conservation of energy and momentum we obtain four equations corresponding to the conservation of each of the components of 4-momentum. They are shown below, combining the conservation equations for the x and y components in a single equation[2].

$$2E = E_3 + E_4 + E_5 \qquad 0 = p_{3z} + p_{4z} + p_{5z} \qquad 0 = \mathbf{q}_3 + \mathbf{q}_4 + \mathbf{q}_5 \tag{1.1}$$

Having imposed these constraints, we are left with eight parameters.

[2]This will be useful later on.

Mass shell conditions

Each of the external (incoming and outgoing) particles lies upon its mass shell. This amounts to the following relation being satisfied for the i^{th} external particle

$$p_{i\mu}p_i^{\mu} = E_i^2 - \mathbf{p}_i \cdot \mathbf{p}_i = E_i^2 - p_{ix}^2 - p_{iy}^2 - p_{iz}^2 = m_i^2$$

This gives us five equations, one for each external particle. However, the two corresponding to the incoming protons are identical, so we effectively only have the four distinct equations shown below.

$$E^2 - p^2 = m_p^2 \qquad E_4^2 - q_4^2 - p_{4z}^2 = m_p^2$$
$$E_3^2 - q_3^2 - p_{3z}^2 = m_p^2 \qquad E_5^2 - q_5^2 - p_{5z}^2 = m_\eta^2$$

Using the mass shell conditions for the three outgoing particles to constrain the system further, we are left with five parameters. We will see later that one of these is physically uninteresting due to the cylindrical symmetry of the setup, leaving just *four* physically relevant quantities that we measure in our experiment.

1.3 Mandelstam variables

Relativistic particle collisions are often analyzed using Mandelstam variables [8]. They are useful in this context because they are Lorentz-invariant, *i.e.* they have the same value in all inertial reference frames. As it turns out, the scattering amplitude is also invariant under Lorentz transformations. For this reason, we will map as many of our relativistic quantities as we can onto these variables. But before we do so, we will introduce the Mandelstam variables through a discussion of 2-2 scattering.

Mandelstam variables in 2-2 scattering

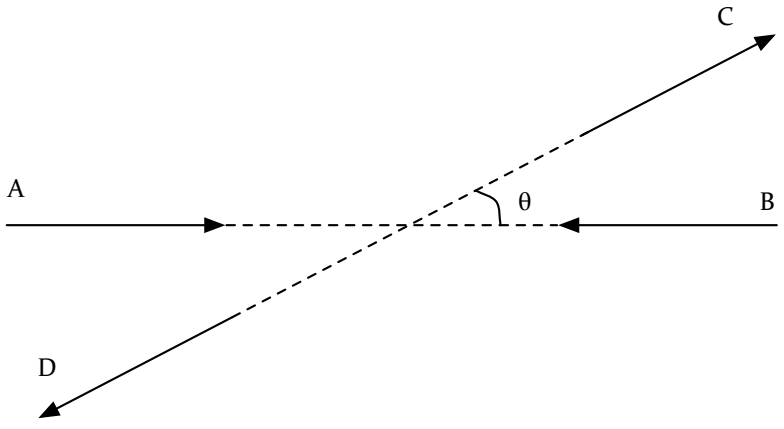

Figure 1.1: 2-2 scattering in the CM frame. Particles A and B collide and are scattered off of each other, becoming particles C and D. The scattering angle in the CM frame is labeled θ (Figure reproduced from [9]).

Figure 1.1 represents the 2-2 scattering process $A + B \rightarrow C + D$. The scattering angle in the CM frame is θ, which satisfies the relation

$$\cos\theta = \frac{\mathbf{p}_A \cdot \mathbf{p}_C}{|\mathbf{p}_A||\mathbf{p}_C|}.$$

The total energy in the CM frame is given by $E_A + E_B$. But we can also write it in the following form.

$$E_A + E_B = \sqrt{(E_A + E_B)^2} = \sqrt{[(E_A, \mathbf{p}_A) + (E_B, \mathbf{p}_B)]^2} = \sqrt{(p_A + p_B)^2}$$

where the second step proceeds because $p_A + p_B = 0$ in the CM frame. The quantity $(p_A + p_B)^2$ is a relativistic scalar product, *i.e.* it is Lorentz-invariant and is represented by the first of our Mandelstam variables, s. Therefore, s measures the total energy in the CM frame.

$$E_A + E_B = E_{total} = \sqrt{s}$$

By conservation of energy, we also have

$$E_A + E_B = E_C + E_D$$

Thus,

$$s = (p_A + p_B)^2 = (p_C + p_D)^2$$

We now introduce two other invariants, t and u, defined below:

$$t = (p_C - p_A)^2 = (p_D - p_B)^2$$
$$u = (p_C - p_B)^2 = (p_D - p_A)^2$$

The variable t measures the momentum transfer in the CM frame and is related to the angle of scattering θ as shown below.

$$t = (p_C - p_A)^2 = (E_C - E_A)^2 - |\mathbf{p}_C - \mathbf{p}_A|^2 = m_C^2 + m_A^2 + 2|\mathbf{p}_C||\mathbf{p}_A|\cos\theta$$

where we have applied the mass shell conditions for particles A and B.

Now, at very high energies, $s >> m_A^2, m_B^2, m_C^2, m_D^2$. In this limit,

$$t \approx \frac{-s}{2}(1 - \cos\theta)$$

Furthermore, if t is fixed, then as s increases, the term $(1 - \cos\theta)$ decreases, that is, $\cos\theta$ tends to 1, implying that θ goes to zero. Thus we see that the large s, fixed t regime corresponds to small-angle scattering at high energies.[3] This is known as the *Regge limit*.

[3]There is a lot more that can be said about and learned from the symmetry between s,t and u in the 2→2 scattering case that is outside the scope of this thesis. For a detailed treatment, see section 1.7 in [9].

Mandelstam variables in 2-3 scattering

Similar to the 2-2 case, we can define the following Mandelstam variables for 2-3 scattering.

$$\begin{aligned} s &= (p_1 + p_2)^2 \\ s_1 &= (p_3 + p_5)^2 & t_1 &= (p_3 - p_1)^2 \\ s_2 &= (p_4 + p_5)^2 & t_2 &= (p_4 - p_2)^2 \end{aligned}$$

where s represents the square of the total energy of the incoming particles in the CM frame, s_1 and t_1 represent the squares of the CM energy and momentum transfer respectivelyin the subsystem containing particle 3 & 5. The variables s_2 and t_2 represent the same quantities, but in the particle 4 & 5 subsystem.

1.4 Mapping our parameters onto Mandelstam variables

We now have an array of equations that we can use to express our physical parameters in terms of Mandelstam variables. We start with the energy of the incoming protons E, which we will obtain from the definition of the Mandelstam variable s.

$$s = (p_1 + p_2)^2 = (2E, 0, 0, 0)^2 = 4E^2 \qquad \Rightarrow \qquad \boxed{E = \frac{\sqrt{s}}{2}} \tag{1.2}$$

The extraction of p from the mass-shell conditions of particles 1 and 2 is also simple.

$$E^2 - p^2 = m_p^2 \qquad \Rightarrow \qquad \boxed{p = \sqrt{\frac{s}{4} - m_p^2}}$$

Expressing E_4 in terms of Mandelstam variables turns out to be a more involved calculation:

$$\begin{aligned} s_1 &= (p_3 + p_5)^2 \\ &= (E_3 + E_5, q_{3x} + q_{5x}, q_{3y} + q_{5y}, p_{3z} + p_{5z})^2 \\ &= (E_3 + E_5)^2 - (\mathbf{q}_3 + \mathbf{q}_5)^2 - (p_{3z} + p_{5z})^2 \\ &= (2E - E_4)^2 - (-\mathbf{q}_4) \cdot (-\mathbf{q}_4) - (-p_{4z}))^2 \\ &= 4E^2 + E_4^2 - 4EE_4 + q_4^2 - p_{4z}^2 \\ &= 4\left(\frac{\sqrt{s}}{2}\right)^2 - 4\left(\frac{\sqrt{s}}{2}\right)E_4 + (E_4^2 + q_4^2 - p_{4z}^2) \\ &= s - 2\sqrt{s}E_4 + m_p^2 \end{aligned}$$

$$\Rightarrow \qquad \boxed{E_4 = \frac{1}{2\sqrt{s}}(s - s_1 + m_p^2)}$$

The other kinematic parameters can be expressed in terms of the Mandelstam variables through similar manipulations, the details of which I have suppressed in the interest of readability. A nearly

identical calculation to the one just performed gives us

$$\boxed{E_3 = \frac{1}{2\sqrt{s}}(s - s_2 + m_p^2)}$$

We can obtain a Lorentz-invariant expression for p_{3z} from the definition of t_1 as shown below.

$$t_1 = (p_3 - p_1)^2 = 2m_p^2 - \frac{(s - s_2 + m_p^2)}{2} + 2p_{3z}p \qquad \Rightarrow \qquad \boxed{p_{3z} = \frac{1}{2\sqrt{\frac{s}{4} - m_p^2}}\left(t_1 + \frac{s - s_2 - 3m_p^2}{2}\right)}$$

The calculation to obtain p_{4z} from the definition $t_2 = (p_4 - p_2)^2$ proceeds similarly, except for a negative sign introduced by the relation $p_2 = -p_1$.

$$\boxed{p_{4z} = \frac{-1}{2\sqrt{\frac{s}{4} - m_p^2}}\left(t_2 + \frac{s - s_1 - 3m_p^2}{2}\right)}$$

From the boxed quantities above, we can calculate E_5 and p_{5z}. From the conservation of energy, we have

$$E_5 = 2E - E_3 - E_4 = \frac{1}{2\sqrt{s}}(2s - 2s + s_1 + s_2 - 2m_p^2) \qquad \Rightarrow \qquad \boxed{E_5 = \frac{1}{2\sqrt{s}}\left(s_1 + s_2 - 2m_p^2\right)}$$

and from the conservation of the z-component of momentum, we get

$$p_{5z} = -(p_{3z} + p_{4z}) = \frac{1}{2p}\left(t_2 - t_1 + \frac{s_2 - s_1}{2}\right) \qquad \Rightarrow \qquad \boxed{p_{5z} = \frac{1}{2\sqrt{\frac{s}{4} - m_p^2}}\left(t_2 - t_1 + \frac{s_2 - s_1}{2}\right)}$$

Now, let us replace q_{5x} and q_{5y} with the composite variables q_5 and θ_5, where q_5 is the length of $\mathbf{q}_5$ and θ_5 the angle between $\mathbf{q_5}$ and the x-axis (See Figure 1.2). That is,

$$q_{5x} = q_5 \cos\theta_5 \qquad\qquad q_{5y} = q_5 \sin\theta_5$$

From the mass shell condition for particle 5 again,

$$q_5^2 = E_5^2 - p_{5z}^2 - m_\eta^2$$

$$\Rightarrow \boxed{q_5 = \sqrt{\left(\frac{1}{2\sqrt{s}}(s_1 + s_2 - 2m_p^2)\right)^2 - \left(\frac{1}{2\sqrt{\frac{s}{4} - m_p^2}}\left(t_2 - t_1 + \frac{s_2 - s_1}{2}\right)\right)^2 - m_\eta^2}}$$

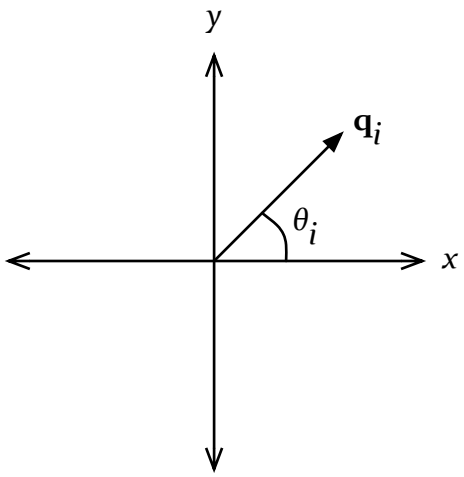

Figure 1.2: A cross section of the beam, showing the projection of the spatial momentum of the i^{th} particle on the $x-y$ plane and the angle it makes with the x-axis

Similarly, we can replace q_{3x}, q_{3y}, q_{4x}, and q_{4y} with q_3, q_4, θ_3 and θ_4 as follows.

$$q_{3x} = q_3 \cos\theta_3 \qquad q_{4x} = q_4 \cos\theta_4$$
$$q_{3y} = q_3 \sin\theta_3 \qquad q_{4y} = q_4 \sin\theta_4$$

where θ_3 and θ_4 are the angles between the vectors $\mathbf{q}_3$ and $\mathbf{q}_4$ and the x-axis. We can get q_3 and q_4 from the mass shell conditions for particles 3 and 4, similar to the way we got q_5 from the mass shell condition for the meson.

$$q_3^2 = E_3^2 - p_{3z}^2 - m_p^2 \qquad q_4^2 = E_4^2 - p_{4z}^2 - m_p^2$$

The above equations give us

$$q_3 = \sqrt{\left(\frac{1}{2\sqrt{s}}(s - s_2 + m_p^2)\right)^2 - \left(\frac{1}{2\sqrt{\frac{s}{4} - m_p^2}}(t_1 + \frac{s - s_2 - 3m_p^2}{2})\right)^2 - m_p^2}$$

$$q_4 = \sqrt{\left(\frac{1}{2\sqrt{s}}(s - s_1 + m_p^2)\right)^2 - \left(\frac{1}{2\sqrt{\frac{s}{4} - m_p^2}}(t_2 + \frac{s - s_1 - 3m_p^2}{2})\right)^2 - m_p^2}$$

We can further combine θ_3 and θ_4 to form the composite variables

$$\theta_{34} = \theta_4 - \theta_3 \qquad \phi = \theta_3 + \theta_4$$

Having done so, we can constrain θ_{34} by manipulating the conservation of momentum relation in the $x-y$ plane[4]

$$\mathbf{q}_5 = -(\mathbf{q}_3 + \mathbf{q}_4) \quad \Rightarrow \quad q_5 = \sqrt{q_3^2 + q_4^2 + 2q_3q_4\cos\theta_{34}} \quad \Rightarrow \quad \boxed{\theta_{34} = \cos^{-1}\left(\frac{q_5^2 - q_4^2 - q_3^2}{2q_3q_4}\right)}$$

The two remaining parameters are θ_5 and ϕ. They depend upon each other, and we can only constrain one of them. However, the remaining unconstrained parameter, whether it is θ_5 or ϕ, turns out to be physically uninteresting because our experiment has cylindrical symmetry: there is no preferred value of θ_{34} or ϕ - the distribution of scattering events is independent of them.

1.5 Approximations in the Regge limit

In the Regge limit for 2-3 scattering,

$$s >> s_1, s_2 >> t_1, t_2, m_p, m_\eta$$

Using the above relations, we can perform leading-order approximations upon our constrained quantities. For p, we have

$$p = \sqrt{\frac{s}{4} - m_p^2} \approx \frac{\sqrt{s}}{2}$$

Performing similar approximations on all our constrained quantities, we obtain the following list of physical quantities expressed in Mandelstam variables in the Regge limit.

$$E = \frac{\sqrt{s}}{2} \qquad p \approx \frac{\sqrt{s}}{2}$$

$$E_3 \approx \frac{s - s_2}{2} \qquad p_{3z} \approx \frac{s - s_2}{2\sqrt{s}} \qquad q_3^2 \approx -t_1$$

$$E_4 \approx \frac{s - s_1}{2} \qquad p_{4z} \approx -\frac{s - s_1}{2\sqrt{s}} \qquad q_4^2 \approx -t_2$$

$$E_5 \approx \frac{s_1 + s_2}{2\sqrt{s}} \qquad p_{5z} \approx \frac{s_2 - s_1}{2\sqrt{s}} \qquad q_5^2 \approx -m_\eta^2$$

[4]We have already constrained q_3, q_4 and q_5, so any quantity expressed in terms of these three quantities is automatically constrained as well.

Chapter 2

Confluence of Theory and Experiment

In this chapter, we will first introduce classical scattering theory and describe how experimentalists actually gather data. We will then proceed to describing scattering in a relativistic quantum mechanical regime. The quantity known as the scattering amplitude is introduced briefly for the first time, before being set aside to focus on bringing the expression for the total scattering cross-section in line with quantities that are measured in the laboratory. The sections on classical scattering theory and the plausibility arguments for Fermi's Golden Rule derive heavily from [6].

2.1 Classical scattering

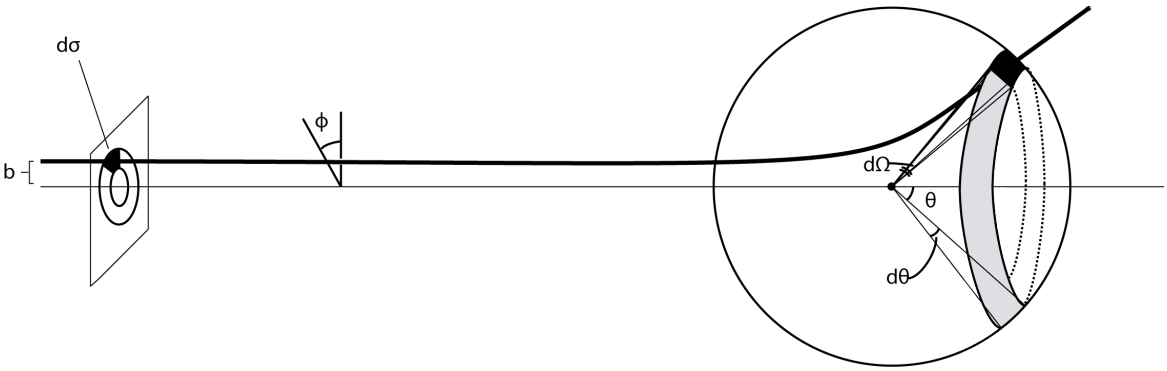

Figure 2.1: Particles incident in the area $d\sigma$ scatter into the solid angle $d\Omega$. (Reproduced from Fig. 6.3 in [6])

We will begin with a simplified model of particle scattering in which we ignore quantum mechanical effects. Figure 2.1 depicts such a process. A particle is initially fired from the left at a stationary target particle situated at the center of a spherical detector chamber. The incoming particle scatters off of the stationary particle at an angle θ and hits a detector located on the interior surface of the chamber. The incident particle and the target particle do not actually need to physically touch to scatter - for example, two electrically charged particles can pass near each other without touching, yet influence each other through the Coulomb force. Essentially, particles that pass through the

infinitesimal cross-sectional area $d\sigma$ scatter into a corresponding infinitesimal solid angle $d\Omega$. The quantity $\frac{d\sigma}{d\Omega}$ is known as the *differential cross-section*. In the scattering process depicted in Fig. 2.1, the differential cross-section is a function of θ, the angle that the scattered particle makes with the z-axis.

$$\frac{d\sigma}{d\Omega} = D(\theta)$$

If the experiment did not possess cylindrical symmetry, then the differential cross-section would depend upon the azimuthal angle ϕ as well. Now, instead of a single particle, consider a beam of particles being fired at the target with luminosity $\mathcal{L}$. The luminosity is a characteristic of the beam - it is the number of particles being fired per unit time per unit cross-sectional area of the beam (not to be confused with the differential cross section). The number of particles passing through $d\sigma$ per unit time is given by

$$dN = \mathcal{L}d\sigma = \mathcal{L}D(\theta)d\Omega$$

This relation is the key to linking theory and experiment. Upon manipulation, we get the relation

$$\frac{d\sigma}{d\Omega} = \frac{dN}{\mathcal{L}d\Omega}$$

If we consider a detector on the inner surface of the sphere that subtends a solid angle $d\Omega$ at the center, then we can measure the differential cross-section by setting the luminosity of the beam and measuring the rate at which particles strike the detector. Another quantity that is often of interest in experimental particle physics is σ, the total cross-section. It is simply the integral of the differential cross-section over all solid angles $d\Omega$.

$$\sigma = \int d\sigma = \int D(\theta)d\Omega$$

It can be thought of as the 'face' that the stationary particle presents to the incoming beam of particles. The total number of particles scattered by the target per unit time is equal to $\mathcal{L}\sigma$. In the following section, we'll see what the differential and total cross-sections look like in a quantum mechanical setting.

2.2 Quantum scattering

In a relativistic quantum mechanical framework, the total scattering cross-section is given by *Fermi's Golden Rule*. For the process where particles 1 and 2 collide to produce particles 3, 4, ..., n

$$1 + 2 \rightarrow 3 + 4 + ... + n$$

the expression for the scattering cross section is given by

$$\sigma = \frac{S\hbar^2}{4\sqrt{(p_1 \cdot p_2)^2 - (m_1 m_2)^2}} \int |\mathcal{M}|^2 (2\pi)^4 \delta^4(p_1 + p_2 - p_3 - \cdots - p_n) \times \prod_{j=3}^{n} (2\pi)\delta\left(p_j^2 - m_j^2\right)\theta\left(p_j^0\right)\frac{d^4 p_j}{(2\pi)^4}$$

The derivation of this arcane expression is beyond the scope of this thesis, however, we can motivate it using a few plausibility arguments.[1] In essence, the Golden Rule instructs us to integrate the differential cross-section over all possible combinations of the 4-momenta of the outgoing particles[2], subject to the kinematic constraints listed below.

1. Every external particle in the process lies on its mass-shell. Thus the terms $\delta(p_j^2 - m_j^2)$.

2. Every outgoing energy (denoted by denoted by p_j^0) is positive. The term $\theta(p_j^0)$ enforces this condition.[3]

3. Energy and momentum are conserved in the process. This is enforced by the delta function $\delta^4(p_1 + p_2 - p_3 - \cdots - p_n)$.

We call this the integral over the *phase-space* of final external momenta. The term $|\mathcal{M}|^2$ makes some combinations of outgoing momenta more probable than others, where $\mathcal{M}$ is the quantum mechanical *scattering amplitude* for this process. We can simplify this expression by integrating over each p_j^0 using the delta function $\delta(p_j^2 - m_j^2)$. This gives us the general expression

$$\sigma = \frac{S\hbar^2}{4\sqrt{(p_1 \cdot p_2)^2 - (m_1 m_2)^2}} \int |\mathcal{M}|^2 (2\pi)^4 \delta^4(p_1 + p_2 - p_3 - \cdots - p_n) \times \prod_{j=3}^{n} \frac{1}{2\sqrt{\mathbf{p}_j^2 + m_j^2}} \frac{d^3\mathbf{p}_j}{(2\pi)^3}$$

with all other instances of p_j^0 in the amplitude $\mathcal{M}$ and the conservation of momentum delta function replaced with $\sqrt{\mathbf{p}_j^2 + m_j^2}$. Applying this formula to our process $p + p \rightarrow p + p + \eta$, we substitute the mass of the proton m_p in place of the masses m_1 and m_2 and replace n by 5, which is the number of particles involved.

$$\sigma = \frac{S\hbar^2}{4\sqrt{(p_1 \cdot p_2)^2 - m_p^4}} \int |\mathcal{M}|^2 (2\pi)^4 \delta^4(p_1 + p_2 - p_3 - p_4 - p_5) \times \prod_{j=3}^{5} \frac{1}{2\sqrt{\mathbf{p}_j^2 + m_j^2}} \frac{d^3\mathbf{p}_j}{(2\pi)^3}$$

We will apply a number of simplifications and change of variable (c.o.v.) operations to this integral to express it in terms of the four parameters that experimentalists measure, t_1, t_2, x_F, and θ_{34}.

2.3 Preliminaries

Before we go ahead and perform the c.o.v. operations, we need to take care of a few things.

Term outside the integral

The first on the list is the term outside the integral:

$$\frac{S\hbar^2}{4\sqrt{(p_1 \cdot p_2)^2 - m_p^4}}$$

[1] If you are curious about the derivation, see Ch. 11 in Srednicki's *Quantum Field Theory* (2007).
[2] Whereas in classical scattering we integrated the differential cross-section over all values of θ and ϕ.
[3] $\theta(p_j^0)$ refers to the Heaviside step function, defined to be 0 when $p_j^0 < 0$ and 1 if $p_j^0 > 0$.

In this term, S is a statistical factor that accounts for identical outgoing particles, and we can write it as follows.

$$S = \prod_{i=1}^{n} \left(\frac{1}{s_i!} \right)$$

for n groups of identical particles with s_i particles in the i^{th} group. For our process, $p + p \rightarrow p + p + \eta$, there are two identical particles (protons) in the final product. Therefore, S is given by

$$S = \left(\frac{1}{2!} \right) = \frac{1}{2}$$

The denominator $4\sqrt{(p_1 \cdot p_2)^2 - m_p^4}$, when expressed in terms of Mandelstam variables, is approximately equal to $2s$ in the Regge limit. Thus the factor outside the integral becomes $\hbar^2/4s$, which after normalizing $\hbar$ to 1 (since we are working in Planck units) itself reduces to $1/4s$.

Integration over $\mathbf{p}_5$

Substituting the values of the 4-momenta of the five particles in the process in the overall conservation of energy and momentum delta function gives us

$$\delta(2E - E_3 - E_4 - E_5)\delta^3(-\mathbf{p}_3 - \mathbf{p}_4 - \mathbf{p}_5)$$

Inserting this back into the integral and simplifying,

$$\sigma = \frac{1}{4s(2\pi)^5} \int |\mathcal{M}|^2 \frac{\delta(2E - E_3 - E_4 - E_5)\delta^3(-\mathbf{p}_3 - \mathbf{p}_4 - \mathbf{p}_5) d\mathbf{p}_3 d\mathbf{p}_4 d\mathbf{p}_5}{\sqrt{\mathbf{p}_3^2 + m_3^2}\sqrt{\mathbf{p}_4^2 + m_4^2}\sqrt{\mathbf{p}_5^2 + m_5^2}}$$

We can take the integral over $\mathbf{p}_5$ immediately using the delta function $\delta(-\mathbf{p}_3 - \mathbf{p}_4 - \mathbf{p}_5)$, replacing $\mathbf{p}_5$ with $-(\mathbf{p}_3 + \mathbf{p}_4)$. Thus, the above expression reduces to:

$$\sigma = \frac{1}{128\pi^5 s} \int |\mathcal{M}|^2 \frac{\delta(2E - E_3 - E_4 - E_5) d\mathbf{p}_3 d\mathbf{p}_4}{\sqrt{\mathbf{p}_3^2 + m_p^2}\sqrt{\mathbf{p}_4^2 + m_p^2}\sqrt{(\mathbf{p}_3 + \mathbf{p}_4)^2 + m_\eta^2}}$$

At this point, we can write $d\mathbf{p}_3 d\mathbf{p}_4$ in an expanded form as $dq_{3x} dq_{3y} dp_{3z} dq_{4x} dq_{4y} dp_{4z}$ and proceed to the change of variable operations.

2.4 Change of variable operations

For our first operation, we will transform this integral over the Cartesian coordinates $\{q_{ix}, q_{iy}\}$ to one over the polar coordinates $\{q_i, \theta_i\}$. By doing this we can exploit some nifty properties of the azimuthal symmetry of our experiment, as well as place ourselves on more familiar ground - recall that we have already expressed q_3, q_4, and q_5 in terms of Mandelstam variables. To transform the integral from the

coordinates $\{q_{ix}, q_{iy}\}$ to the coordinates $\{q_i, \theta_i\}$, we make the substitution in the integrand:

$$dq_{ix}, dq_{iy} \rightarrow dq_i d\theta_i |\det J|$$

where J is the Jacobian matrix for the mapping $\{q_i, \theta_i\} \rightarrow \{q_{ix}, q_{iy}\}$.[4] For this transformation, we have

$$J = \begin{pmatrix} \frac{\partial q_{ix}}{\partial q_i} & \frac{\partial q_{ix}}{\partial \theta_i} \\ \frac{\partial q_{iy}}{\partial q_i} & \frac{\partial q_{iy}}{\partial \theta_i} \end{pmatrix} = \begin{pmatrix} \frac{\partial (q_i \cos\theta_i)}{\partial q_i} & \frac{\partial (q_i \cos\theta_i)}{\partial \theta_i} \\ \frac{\partial (q_i \sin\theta_i)}{\partial q_i} & \frac{\partial (q_i \sin\theta_i)}{\partial \theta_i} \end{pmatrix} = \begin{pmatrix} \cos\theta_i & -q_i \sin\theta_i \\ \sin\theta_i & q_i \cos\theta_i \end{pmatrix}$$

and its determinant is $|\det J| = q_i$. Thus, $dq_{ix} dq_{iy}$ gets replaced by $q_i dq_i d\theta_i$, along with an appropriate change of integration limits. The rest of the change of variable operations will proceed similarly - we will essentially calculate the determinants of a few Jacobian matrices.

Change of variables from $\{p_{3z}, p_{4z}\}$ to $\{x_F, s_T\}$

Next, we transform the integral over the coordinates $\{p_{3z}, p_{4z}\}$ to one over the coordinates $\{x_F, s_T\}$ where

$$x_F = -\frac{p_{3z} + p_{4z}}{p} \qquad \text{and} \qquad s_T = s_1 + s_2$$

The variable x_F is an experimentally measured quantity that represents the ratio of the z-component of momentum of the η meson to the magnitude of the z-component of the momentum of either of the two incoming protons, and s_T is a composite variable that we will eliminate using the energy conservation delta function. Before we construct the Jacobian for the transformation $\{p_{3z}, p_{4z}\} \rightarrow \{x_F, s_T\}$, let us express x_F in terms of Mandelstam variables.

$$x_F = -\frac{p_{3z} + p_{4z}}{p} \approx \frac{s_2 - s_1}{s} \qquad \Rightarrow \qquad s x_F = s_2 - s_1$$

Using the above and the definition of s_T, we can write p_{3z} and p_{4z} as shown below:

$$p_{3z} = \frac{1}{4\sqrt{s}}(2s - s_T - s x_F) \qquad \text{and} \qquad p_{4z} = \frac{1}{4\sqrt{s}}(2s - s_T + s x_F)$$

We can now calculate the determinant of the Jacobian matrix for the mapping $\{x_F, s_T\} \rightarrow \{p_{3z}, p_{4z}\}$ as shown below:

$$\begin{vmatrix} \frac{\partial p_{3z}}{\partial x_F} & \frac{\partial p_{3z}}{\partial s_T} \\ \frac{\partial p_{4z}}{\partial x_F} & \frac{\partial p_{4z}}{\partial s_T} \end{vmatrix} = \begin{vmatrix} \frac{1}{4\sqrt{s}}(-s) & \frac{1}{4\sqrt{s}}(-1) \\ \frac{1}{4\sqrt{s}}(s) & \frac{1}{4\sqrt{s}}(-1) \end{vmatrix} = \frac{1}{8}$$

And so we make the replacement

$$dp_{3z} dp_{4z} \rightarrow \frac{1}{8} dx_F ds_T$$

[4] This result arises from multivariate calculus and the change of variable theorem.

Change of variables from $\{\theta_3, \theta_4\}$ to $\{\theta_{34}, \phi\}$

We now perform a change of variable operation to transform from the $\{\theta_3, \theta_4\}$ coordinate system to the $\{\theta_{34}, \phi\}$ system, where

$$\theta_{34} = \theta_4 - \theta_3 \qquad \text{and} \qquad \phi = \theta_4 + \theta_3.$$

To facilitate the construction of the Jacobian matrix, we can write θ_3 and θ_4 in terms of θ_{34} and ϕ as follows:

$$\theta_3 = \frac{1}{2}(\phi - \theta_{34}) \qquad \text{and} \qquad \theta_4 = \frac{1}{2}(\phi + \theta_{34}).$$

$|\det J|$ for the mapping $\{\theta_{34}, \phi\} \to \{\theta_3, \theta_4\}$ is then given by

$$\begin{vmatrix} \frac{\partial\theta_3}{\partial\theta_{34}} & \frac{\partial\theta_3}{\partial\phi} \\ \frac{\partial\theta_4}{\partial\theta_{34}} & \frac{\partial\theta_4}{\partial\phi} \end{vmatrix} = \begin{vmatrix} \frac{1}{2}(-1) & \frac{1}{2}(1) \\ \frac{1}{2}(1) & \frac{1}{2}(1) \end{vmatrix} = \frac{1}{2}$$

Thus we make the substitution

$$d\theta_3 d\theta_4 \to \frac{1}{2} d\theta_{34} d\phi$$

Change of variables from $\{q_3, q_4\}$ to $\{t_1, t_2\}$

We can perform our last change of variable operation quickly and without constructing the Jacobian matrix first. From our Mandelstam variable approximations in the Regge limit,

$$q_3^2 \approx -t_1 \Rightarrow 2q_3 dq_3 \approx -dt_1$$

Similarly, $2q_4 dq_4 \approx -dt_2$. From these two relations we can determine the substitution needed for this change of variables, which turns out to be

$$q_3 dq_3 q_4 dq_4 \to \frac{1}{4} dt_1 dt_2$$

Putting it all together

Phew. We are finally done! After combining the results of all the c.o.v. operations, we can sit back and admire the end result of our efforts, that is, the overall substitution

$$dq_{3x} dq_{3y} dp_{3z} dq_{4x} dq_{4y} dp_{4z} \to \frac{1}{64} dt_1 dt_2 dx_F ds_T d\theta_{34} d\phi$$

We won't sit for long, though. We will move on to the following section in which we will get rid of the dependence on ϕ and s_T. This will leave us with a cross-section and associated differential cross section that depend only upon the variables t_1, t_2, x_F and θ_{34}.

2.5 Integrating over ϕ and s_T

From the mass shell condition for particle 5,

$$E_5 = \sqrt{\mathbf{p}_5^2 + m_\eta^2}$$

Since we already integrated over the delta function that set $\mathbf{p}_5 = -(\mathbf{p}_3 + \mathbf{p}_4)$, we have

$$E_5 = \sqrt{E_3^2 - m_p^2 + E_4^2 - m_p^2 + 2(q_3 q_4 \cos\theta_{34} + p_{3z}p_{4z}) + m_\eta^2}$$

Since the term q_3q_4 is on the order of t_1 and t_2, we can take it to be negligible in the Regge limit along with the masses. Thus,

$$E_5 \approx \frac{s|x_F|}{2\sqrt{s}} \tag{2.1}$$

We can therefore write the delta function $\delta(2E - E_3 - E_4 - E_5)$ in terms of s and s_T as follows.

$$\delta(2E - E_3 - E_4 - E_5) = \delta\left(\frac{s_T - s|x_F|}{2\sqrt{s}}\right) \tag{2.2}$$

Then, we can use Equation 2.1 and Equation 2.2 to rewrite the integral as

$$\sigma = \frac{1}{8192\pi^5 s}\int |\mathcal{M}|^2 \frac{\delta\left(\frac{s_T - s|x_F|}{2\sqrt{s}}\right)(2\sqrt{s})dt_1dt_2dx_Fds_Td\theta_{34}d\phi}{\sqrt{\mathbf{p}_3^2 + m_p^2}\sqrt{\mathbf{p}_4^2 + m_p^2}(s|x_F|)}$$

We can perform the integral over ϕ immediately since our system has cylindrical symmetry and none of the other terms depend on ϕ - this results in a factor of 2π outside the integral. Putting this factor in along with expressing the rest of the quantities in terms of Mandelstam variables gives us

$$\sigma = \frac{1}{4096\pi^4 s}\int |\mathcal{M}|^2 \frac{\delta\left(\frac{s_T - s|x_F|}{2\sqrt{s}}\right)s\sqrt{s}dt_1dt_2dx_Fds_Td\theta_{34}}{\left(s - \frac{s_T + sx_F}{2}\right)\left(s - \frac{s_T - sx_F}{2}\right)(s|x_F|)}$$

We can immediately perform the integral with respect to s_T due to the presence of the delta function containing it, thereby removing the delta function and replacing all instances of s_T by $s|x_F|$.

$$\sigma = \frac{1}{4096\pi^4 s}\int |\mathcal{M}|^2 \frac{s\sqrt{s}dt_1dt_2dx_Fd\theta_{34}}{\left(s - \frac{s|x_F| + sx_F}{2}\right)\left(s - \frac{s|x_F| - sx_F}{2}\right)(s|x_F|)} \tag{2.3}$$

The term $\mathcal{M}$ now refers to the form of the amplitude where all the dependence on the kinematic parameters has been expressed in terms of the four unconstrained, physically measured quantities t_1, t_2, x_F and θ_{34} The presence of $|x_F|$ splits the expression into two forms, one for $x_F \leq 0$ and the

other for $x_F \geq 0$. We know that

$$|x_F| = \begin{cases} x_F & \forall x_F \geq 0 \\ -x_F & \forall x_F \leq 0 \end{cases}$$

Substituting these values into Equation 2.3 and simplifying, we get the final form of the total cross section:

$$\sigma = \begin{cases} \int \left(\dfrac{|\mathcal{M}_{\text{mod}}|^2}{4096\pi^4 s^2 \sqrt{s}(1-x_F)(x_F)} \right) dt_1 dt_2 dx_F d\theta_{34} & \forall x_F \geq 0 \\ \\ \int \left(\dfrac{-|\mathcal{M}_{\text{mod}}|^2}{4096\pi^4 s^2 \sqrt{s}(1+x_F)(x_F)} \right) dt_1 dt_2 dx_F d\theta_{34} & \forall x_F \leq 0 \end{cases}$$

The term in the brackets is the differential cross-section:

$$\boxed{\frac{d\sigma}{dt_1 dt_2 dx_F d\theta_{34}} = \left(\frac{|\mathcal{M}_{\text{mod}}|^2}{4096\pi^4 s^2 \sqrt{s}(1-|x_F|)|x_F|} \right)}$$

The differential cross-section can be interpreted as a probability distribution for scattering events. It tells us which scattering events (corresponding to combinations of t_1, t_2, x_F and θ_{34}) are more likely to occur than others - and thus will be detected more often.

Chapter 3

Construction of the Reggeon

This is a fairly long and complicated chapter, so it is worth our while to quickly recap some of the discussion from the introduction as well as present a bird's-eye view of the (often winding) road ahead. Recall that the action of the strong force at ranges exceeding the diameter of hadrons can be modeled as being mediated through the exchange of mesons, similar to the way the electric force is mediated by the exchange of photons and the weak force by the exchange of W and Z bosons. Any meson exchange that satisfies the right quantum number relations among the particles involved is possible. Thus, any process mediated by the exchange of a π^0 meson can also be mediated by the exchange of any one of a family of similar mesons, possessing similar properties but different masses and spins, which we label $\pi^1, \pi^2 \ldots$ and so on. It can also be mediated by the exchange of other families of mesons, such as the ρ and ω mesons. The process $p + p \rightarrow p + p + \eta$, mediated by the exchange of neutral pions, is common at low energies. However, at high energies it is not only the exchange of the spin-0 neutral pion that contributes to the scattering process, but higher spin pions as well. The known neutral pions are represented in Figure 3.1 on a Chew-Frautschi plot. we see that certain members of this family, in particular those with even spin, lie roughly on a straight line. The linear function that describes this is known as the *Regge trajectory*. At high energies it is not enough to consider the contribution of just the spin-0 pion, we must consider the contribution of the entire family. However, it is the members that lie along the Regge trajectory that will contribute the most to the scattering amplitude $\mathcal{M}$. It is for this reason that such processes are said to be mediated by the exchange of Regge trajectories rather than individual particles.

Before we examine the process $p + p \rightarrow p + p + \eta$, let us consider a simpler case, $p + p \rightarrow p + p$, where the process is mediated by the exchange of neutral pions. The total scattering amplitude for the process is found by summing up the amplitudes from the various processes involving the exchange of different members of the neutral pion family. In quantum field theory, scattering amplitudes are found by evaluating the *Feynman diagrams* for the relevant processes. In this case, we would have to evaluate an infinite number of them, which we do *not* want to do. What we will do instead is model the exchange of the entire family of even-spin neutral pions as that of a single fictitious particle called the *Reggeon*. In this chapter, we will first obtain an expression that allows us to substitute a Reggeon in place of a spin-0 pion, by examining 2-2 proton/proton scattering processes. Once we have this

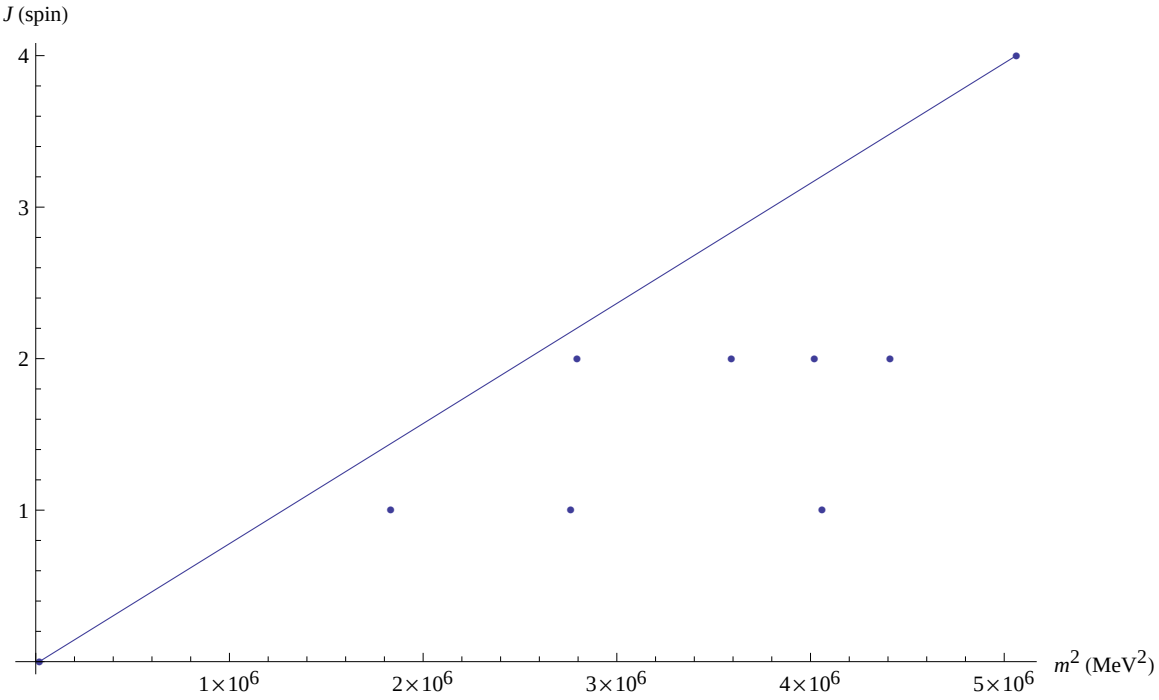

Figure 3.1: A plot of spin vs. mass squared of the family of neutral pions. It is observed that a number of particles lie roughly on a straight line, the Regge trajectory.

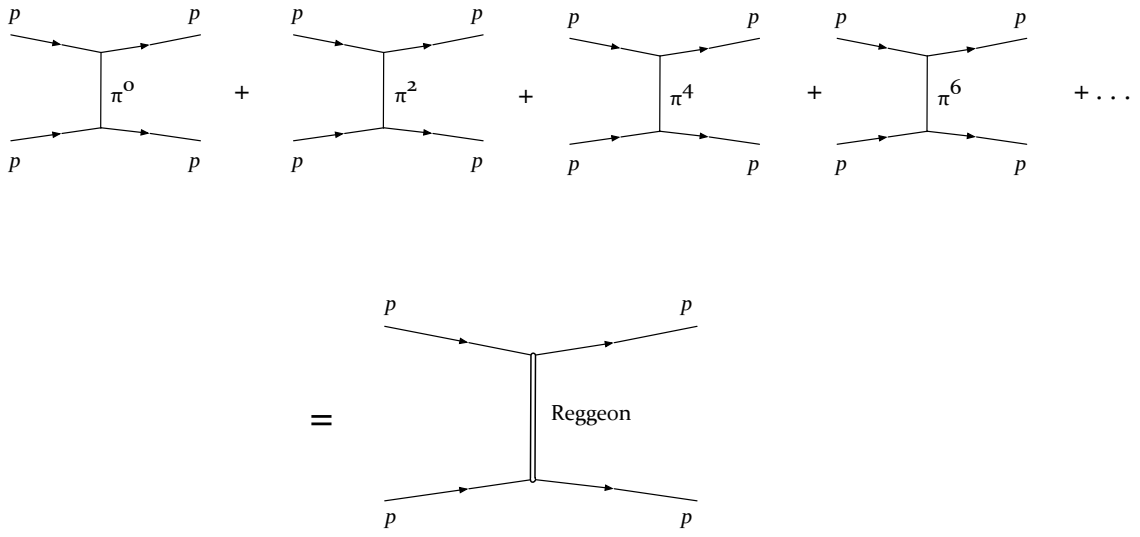

Figure 3.2: The diagram involving the exchange of a Reggeon is equivalent to the collection of diagrams involving the exchange of pions of various spins.

expression, the 'Reggeized propagator', we will evaluate the Feynman diagram for our 2-3 scattering process assuming the exchange of spin-0 pions. Then we will substitute the Reggeized propagator in place of the spin-0 propagator to recover the contribution of the entire family of pions (Figure 3.3).

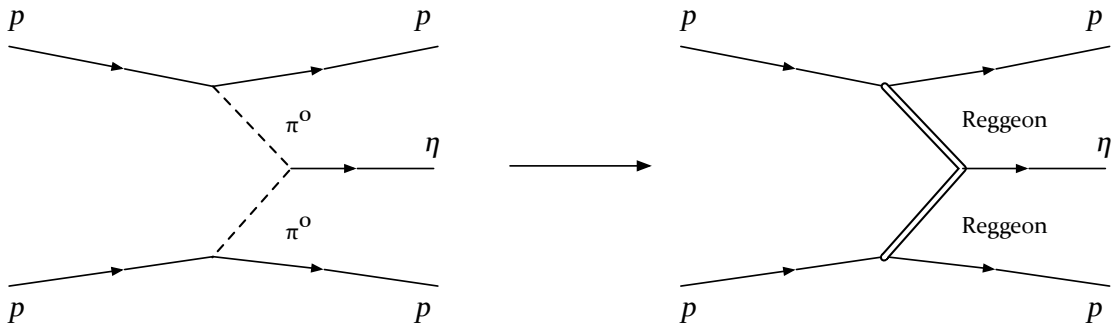

Figure 3.3: We will replace the spin-0 pion propagators in the left Feynman diagram with the Reggeized propagators in the right one.

3.1 Feynman amplitudes

Feynman diagrams are representations of particle interactions. There are a number of rules associated with drawing them and evaluating them that can be derived from quantum field theory, but this derivation is beyond the scope of this thesis. Take for example the Feynman diagram in Figure 3.4. Scan the diagram horizontally across the page from left to right - this represents the direction of time. Thus, the diagram represents two incoming protons exchanging a spin-0 meson and scattering. To

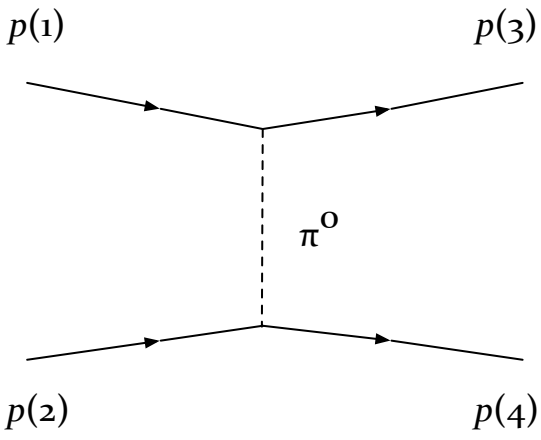

Figure 3.4: Feynman diagram for 2-2 proton-proton scattering with scalar pion propagator. $p(i)$ denotes the i^{th} particle.

calculate the Feynman amplitude $\mathcal{M}$ from this diagram, we apply the *Feynman rules*. These yield

$$\mathcal{M} = \int [\bar{u}_3(-ig_0)u_1]\frac{i}{q_{\pi^0}^2 - m_{\pi^0}^2}[\bar{u}_4(-ig_0)u_2](2\pi)^4\delta^4(p_1 - q_{\pi^0} - p_3)(2\pi)^4\delta^4(p_2 + q_{\pi^0} - p_4)\frac{d^4q_{\pi^0}}{(2\pi)^4}$$

where u_i denotes the spinor[1] and $\bar{u}_i$ the adjoint spinor of the i^{th} particle. We can see how this goes: traveling along the fermion line at the top we pick up a factor of $[\bar{u}_3(-ig_0)u_1]$, where g_0 is the coupling constant associated with this particular 'spinor-scalar-spinor' vertex. Traveling downward, we pick up a factor of $\frac{i}{q_{\pi^0}^2 - m_{\pi^0}^2}$ from the scalar pion propagator (q_{π^0} is the momentum of the pion), and finally another 'sandwich' factor $[\bar{u}_4(-ig_0)u_2]$ from the bottom fermion line. At the end we append the delta functions denoting conservation of momentum at the vertices and the factor $\frac{d^4q_{\pi^0}}{(2\pi)^4}$ indicating integration over the momentum of the exchanged particle. Particles 1 and 2 are the incoming and particles 3 and 4 the outgoing protons. We can perform the integral immediately using the delta function, substituting $(p_1 - p_3)$ for every instance of q_{π^0} and simplify the expression to get

$$\mathcal{M} = (2\pi)^4[\bar{u}_3u_1]\frac{i^3g_0^2}{(p_1 - p_3)^2 - m_{\pi^0}^2}[\bar{u}_4u_2]\delta^4(p_1 + p_2 - p_3 - p_4)$$

The final step is to erase the factor $(2\pi)^4\delta^4(p_1 + p_2 - p_3 - p_4)$ and multiply by i. This leaves us with

$$\mathcal{M} = \frac{g_0^2}{(p_1 - p_3)^2 - m_{\pi^0}^2}[\bar{u}_3u_1][\bar{u}_4u_2] \tag{3.1}$$

At this point we will use the Mandelstam variables s, t and u corresponding to 2-2 scattering discussed in section 1.3. As before, s corresponds to the total energy in the CM frame while t represents the momentum transfer along the internal line in the Feynman diagram. Substituting t for $(p_3 - p_1)^2$ in Equation 3.1, we obtain

$$\mathcal{M} = \frac{g_0^2}{t - m_{\pi^0}^2}[\bar{u}_3u_1][\bar{u}_4u_2]$$

Casimir's Trick

We apply a technique known as Casimir's trick in which we average over the initial spins and sum over the final spins, by which we calculate the spin-averaged amplitude $\langle|\mathcal{M}|\rangle$. This is a more relevant quantity for us because in the actual experiment we are not concerned with the individual spins of the particles in the beams that are collided. To do this, we first square the absolute value of the scattering amplitude as shown below.

$$|\mathcal{M}|^2 = \frac{g_0^4}{(t - m_{\pi^0}^2)^2}[\bar{u}_3u_1]^*[\bar{u}_4u_2]^*[\bar{u}_3u_1][\bar{u}_4u_2]$$

We see that we have terms that have the structure$[\bar{u}_iu_j][\bar{u}_iu_j]^*$ in our amplitude. The average over the initial spins gives us $\frac{1}{4}\sum_{\text{initial spins}}$ since there are two particles, each with two possible spin configu-

[1]Spinors represent solutions of the Dirac equation, which is the relativistic analogue of the Schrödinger equation for spin-1/2 particles.

rations, while the sum over the final spins is simply $\sum_{\text{final spins}}$. Thus, we will have

$$\frac{1}{4}\sum_{\text{all spins}}|\mathcal{M}|^2 = \frac{g_0^4}{4(t-m_{\pi^0}^2)^2}\left[\sum_{\text{spins}}[\bar{u}_3 u_1]^*[\bar{u}_3 u_1]\right]\left[\sum_{\text{spins}}[\bar{u}_4 u_2]^*[\bar{u}_4 u_2]\right] \tag{3.2}$$

Summing over the final spins introduces terms that are simply the traces of matrices, and follow the set of rules known as 'trace theorems', as shown below.[2,3]

$$\sum_{\text{all spins}}[\bar{u}_i u_j][\bar{u}_i u_j]^* = \text{Tr}[(\not{p}_i + m_i)(\not{p}_j + m_j)] \tag{3.3}$$

Substituting Equation 3.3 in Equation 3.2 gives us

$$\langle|\mathcal{M}|^2\rangle = \frac{4g_0^4}{(t-m_{\pi^0}^2)^2}(p_3\cdot p_1 + m_p^2)(p_4\cdot p_2 + m_p^2) \tag{3.4}$$

Now, we know that

$$(p_3 - p_1)^2 = p_3^2 + p_1^2 - 2p_3\cdot p_1 \qquad \Rightarrow \qquad t = m_p^2 + m_p^2 - 2p_3\cdot p_1$$

applying the mass shell conditions. This implies that $p_3\cdot p_1 = m_p^2 - t/2$. Similarly, it can be shown that $p_4\cdot p_2 = m_p^2 - t/2$. Therefore,

$$\boxed{\langle|\mathcal{M}|^2\rangle = \frac{4g_0^4}{(t-m_{\pi^0}^2)^2}\left(2m_p^2 - \frac{t}{2}\right)^2} \tag{3.5}$$

There is another diagram that contributes to this process - one that is identical to the first, but with crossed fermion lines, shown in Figure 3.5 The second diagram differs from the first in that p_3 and p_4

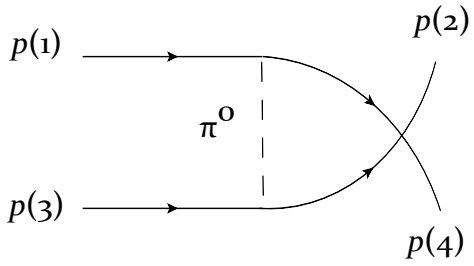

Figure 3.5: Feynman diagram for $p + p \rightarrow p + p$ scattering, mediated by the exchange of a spin-0 pion, with crossed fermion lines.

[2]The derivation of this result can be found in [6], pp. 250-251, albeit with the gamma matrices (γ^μ) that come along with the exchange of spin-1 photons in quantum electrodynamics.

[3]Here we use the Feynman 'slash' notation, where $\not{p} = p^\mu\gamma_\mu$.

are interchanged. This amounts to interchanging the Mandelstam variables t and u, so that

$$\boxed{\langle|\mathcal{M}_{\text{crossed}}|^2\rangle = \frac{4g_0^4}{(u-m_{\pi 0}^2)^2}\left(2m_p^2 - \frac{u}{2}\right)^2}$$

We have just evaluated our first Feynman diagrams! Let us move on to a slightly more involved example.

Vector pion propagator

We will now calculate the scattering amplitudes for the crossed and uncrossed diagrams for the same process, but this time with a spin-1 pion exchanged. The nonzero spin introduces additional complexity in the form of gamma matrices. We can construct the Feynman amplitude for the diagram in

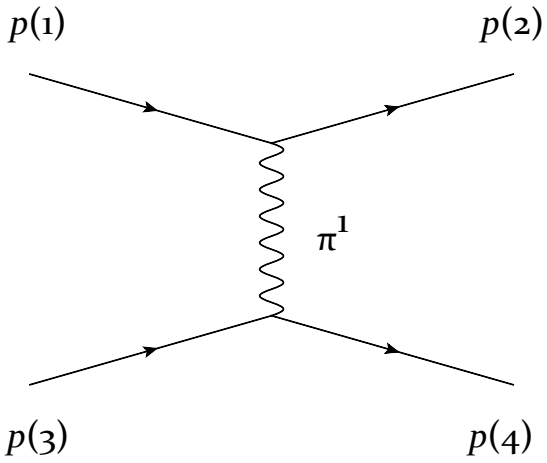

Figure 3.6: Proton/proton scattering through the exchange of a spin-1 pion.

Figure 3.6 similar to the previous example, but with a few changes to the Feynman rules.

1. The coupling constants ig_0 will be replaced by the factor $ig_1\gamma^\mu$ to account for the spinor-vector-spinor vertex that replaces the spinor-scalar-spinor vertex[4].

2. The factor from the vector pion propagator will be $\dfrac{ig_{\mu\nu}}{q_{\pi 1}^2 - m_{\pi 1}^2}$ instead of $\dfrac{i}{q_{\pi 0}^2 - m_{\pi 0}^2}$, where $g_{\mu\nu}$ is the Minkowski metric.

[4]The terms γ^μ refer to 4×4 matrices. In block notation:

$$\gamma^0 = \begin{pmatrix} 1 & 0 \\ 0 & -1 \end{pmatrix} \qquad \gamma^i = \begin{pmatrix} 0 & \sigma^i \\ -\sigma^i & 0 \end{pmatrix}$$

where 1 denotes the 2×2 unit matrix, 0 denotes a 2×2 matrix of zeroes, and σ^i denotes the appropriate Pauli spin matrix.

$$\sigma_x = \sigma^1 = \begin{pmatrix} 0 & 1 \\ 1 & 0 \end{pmatrix} \qquad \sigma_y = \sigma^2 = \begin{pmatrix} 0 & -i \\ i & 0 \end{pmatrix} \qquad \sigma_z = \sigma^3 = \begin{pmatrix} 1 & 0 \\ 0 & -1 \end{pmatrix}$$

Applying the Feynman rules with these modifications, we get the Feynman amplitude

$$\mathcal{M} = \int [\bar{u}_3(ig_1\gamma^\mu)u_1]\frac{ig_{\mu\nu}}{q_{\pi^1}^2 - m_{\pi^1}^2}[\bar{u}_4(ig_1\gamma^\nu)u_2](2\pi)^4\delta^4(p_1^\mu - q_{\pi^1} - p_3^\mu)(2\pi)^4\delta^4(p_2^\mu + q_{\pi^1}^\mu - p_4^\mu)\frac{d^4q_{\pi^1}}{(2\pi)^4}$$

Carrying out the delta function integral over $d^4q_{\pi^1}$, erasing the final overall conservation of momentum factor of $(2\pi)^4\delta^4(p_1 + p_2 - p_3 - p_4)$, and multiplying by i, we have

$$\mathcal{M} = \frac{i^4 g_1^2}{(p_1 - p_3)^2 - m_{\pi^1}^2}[\bar{u}_3\gamma^\mu u_1][\bar{u}_4\gamma_\mu u_2]$$

and averaging over initial spins and summing over final spins yields

$$\begin{aligned}\langle|\mathcal{M}|^2\rangle &= \frac{1}{4}\sum_{\text{all spins}}\frac{g_1^4}{(t - m_{\pi^1}^2)^2}[\bar{u}_3\gamma^\mu u_1]^*[\bar{u}_4\gamma_\mu u_2]^*[\bar{u}_3\gamma^\nu u_1][\bar{u}_4\gamma_\nu u_2] \\ &= \frac{g_1^4}{4(t - m_{\pi^1}^2)^2}\text{Tr}[\gamma^\mu(\not{p}_1 + m_p)\gamma^\nu(\not{p}_3 + m_p)]\text{Tr}[\gamma^\mu(\not{p}_1 + m_p)\gamma^\nu(\not{p}_3 + m_p)]\end{aligned}$$

Evaluating the first trace using the trace theorems gives

$$\text{Tr}[\gamma^\mu(\not{p}_1 + m_p)\gamma^\nu(\not{p}_3 + m_p)] = 4[p_1^\mu p_3^\nu + p_3^\mu p_1^\nu + g^{\mu\nu}(m_p^2 - p_1 \cdot p_3)]$$

Similarly, the second trace is calculated to be $4[p_{2\mu}p_{4\nu} + p_{4\mu}p_{2\nu} - g_{\mu\nu}(m_p^2 - p_2 \cdot p_4)]$. Therefore, $\langle|\mathcal{M}|^2\rangle$ simplifies to

$$\langle|\mathcal{M}|^2\rangle = \frac{4g_1^4}{(t - m_{\pi^1}^2)^2}2[(p_1 \cdot p_2)(p_3 \cdot p_4) + (p_1 \cdot p_4)(p_3 \cdot p_2) + m_p^2(p_1 \cdot p_3 + p_2 \cdot p_4) + 2m_p^4] \tag{3.6}$$

We already know that

$$\boxed{p_3 \cdot p_1 = p_4 \cdot p_2 = m_p^2 - \frac{t}{2}} \tag{3.7}$$

We similarly obtain $(p_1 \cdot p_2)$, $(p_3 \cdot p_4)$, $(p_1 \cdot p_4)$, and $(p_3 \cdot p_2)$ in terms of Mandelstam variables as shown below.

$$\boxed{p_1 \cdot p_2 = p_3 \cdot p_4 = \frac{s}{2} - m_p^2} \quad \text{and} \quad \boxed{p_1 \cdot p_4 = p_3 \cdot p_2 = m_p^2 - \frac{u}{2}} \tag{3.8}$$

Substituting the boxed results from Equation 3.7 and Equation 3.8 into the expression for $\langle|\mathcal{M}|^2\rangle$ in Equation 3.6, and simplifying, we have

$$\boxed{\langle|\mathcal{M}|^2\rangle = \frac{2g_1^4(s^2+u^2+8m_p^4)}{\left(t-m_{\pi^1}^2\right)^2}} \tag{3.9}$$

To get $\langle|\mathcal{M}_{\text{crossed}}|^2\rangle$, we simply switch particles 3 and 4 in the Feynman diagram, as shown in Figure 3.7. Calculating $\langle|\mathcal{M}_{\text{crossed}}|^2\rangle$ by taking Equation 3.9 and interchanging t and u we get

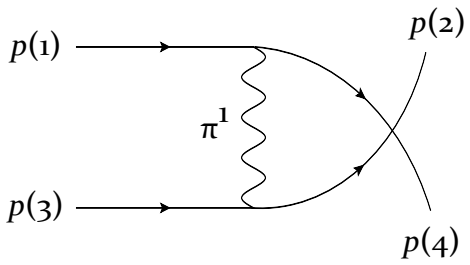

Figure 3.7: Feynman diagram with crossed fermion lines.

$$\boxed{\langle|\mathcal{M}_{\text{crossed}}|^2\rangle = \frac{8g_1^4(s^2+t^2+8m_p^4)}{\left(u-m_{\pi^1}^2\right)^2}}$$

Negligibility of Feynman diagrams with crossed fermion lines.

Recall that we are trying to sum the contributions of 2→2 scattering processes involving the exchanges of pions with increasing spin. We are in the process of showing that we can neglect the contributions of the Feynman diagrams with crossed fermion lines. We can use the relation $s+t+u=4m_p^2$ to write $\langle|\mathcal{M}|^2\rangle$ and $\langle|\mathcal{M}_{\text{crossed}}|^2|\rangle$ as shown below.

$$\langle|\mathcal{M}|^2\rangle = \frac{8g_1^4(s^2+(4m_p^2-s-t)^2+8m_p^4)}{\left(t-m_{\pi^1}^2\right)^2} \tag{3.10}$$

$$\langle|\mathcal{M}_{\text{crossed}}|^2\rangle = \frac{8g_1^4(s^2+t^2+8m_p^4)}{\left(u-m_{\pi^1}^2\right)^2} \tag{3.11}$$

In high energy, small angle deflection scattering processes, s is very large and t is fixed (see section on Mandelstam variables in 2-2 scattering in chapter 1). In order to keep t finite as $s\to\infty$ while

maintaining the relation $s + t + u = 4m_p^2$, u must become very large and negative to compensate. This means that $\langle|\mathcal{M}|^2\rangle$ will become large while $\langle|\mathcal{M}_{\text{crossed}}|^2\rangle$ remains finite, implying that the contribution of the Feynman diagram with crossed fermion lines to the scattering amplitude will be negligible compared to the contribution of the diagram with uncrossed outgoing fermion lines. This result is consistent with the amplitudes from diagrams with higher spin propagators as well - thus we can concentrate on the uncrossed diagrams for our overall scattering amplitude.

We can extrapolate from the spin-0 and spin-1 cases and see that the full amplitude must be a sum of the form

$$\mathcal{M} = \mathcal{M}_{\pi^0} + \mathcal{M}_{\pi^2} + \mathcal{M}_{\pi^4} + \cdots = \frac{f_1(s,t)}{t - m_{\pi^0}^2} + \frac{f_2(s,t)}{t - m_{\pi^2}^2} + \frac{f_3(s,t)}{t - m_{\pi^4}^2} + \ldots \tag{3.12}$$

where the terms f_i are functions of s and t. Note that the total sum is a function with an infinite series of singularities or 'poles' at $t = m_{\pi^i}^2$.

We already know of a function with an infinite series of poles in it - the Gamma function (Γ), depicted in Figure 3.8[5]. It turns out that there is a certain combination of Gamma functions that

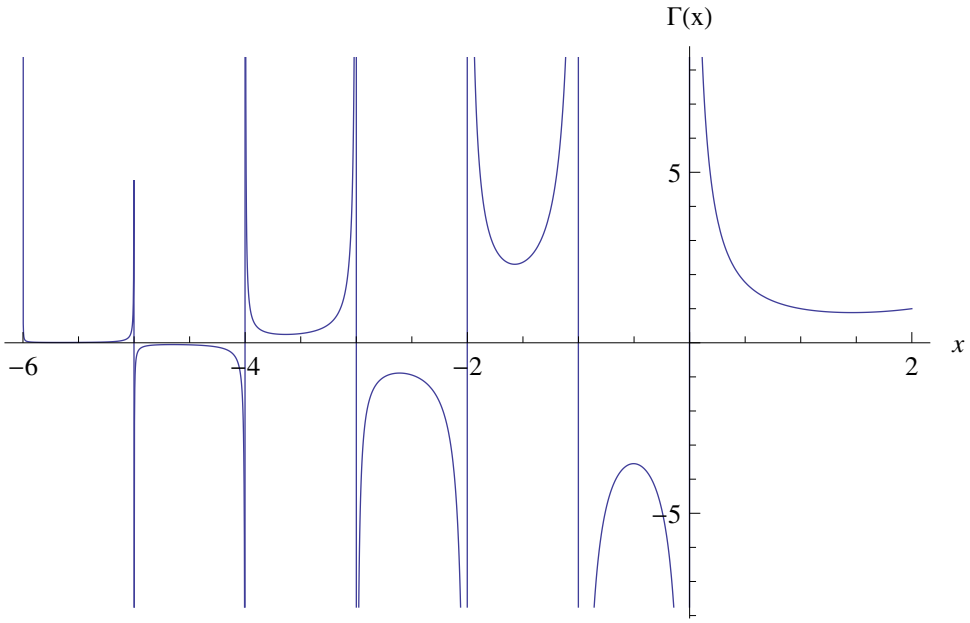

Figure 3.8: The gamma function $\Gamma(x)$ plotted on the domain $x \in (-6, 2)$. Note the singularities at negative integer values of x.

exactly reproduces the pole structure in Equation 3.12. It is known as the *Veneziano amplitude*.

[5]The generalized Gamma function $\Gamma(z)$ is an extension of the factorial to complex number arguments. It is analytic everywhere except for negative integral values of z, that is, for $z \in \{0, -1, -2, -3, \ldots\}$

3.2 Veneziano amplitude

In 1968, Gabriele Veneziano proposed the following expression to describe the high energy behavior of the scattering amplitude of the process $\pi + \pi \rightarrow \pi + \omega$ [13].

$$\mathcal{A}(s,t) = \frac{\Gamma(-\alpha(t))\Gamma(\alpha(s))}{\Gamma(-\alpha(t)-\alpha(s))} K_0(p_1,p_2,p_3,p_4,p_5)$$

This is a function that contains poles in s as well as t, desirable because of a feature known as crossing symmetry. $K_0(p_1,p_2,p_3,p_4,p_5)$ is a kinematic prefactor that does not contain any singularities or zeros and depends on the momenta and polarizations of the scattered particles. This form of the amplitude was successful in describing a large number of high energy scattering processes.

An interesting aside: the Veneziano amplitude was originally a purely phenomenological expression, developed to match the pole structure of the overall scattering amplitude. However, it turned out that this expression emerges from string theory when considering scattering through the exchange of open strings, leading to the idea of modeling the Reggeon as an open string. The derivation of the Veneziano amplitude from string theory can be found in [11].

Pole structure

In this section we will explicitly show that the Veneziano amplitude has the correct pole structure required to model the scattering amplitude.

Because we are working in Planck units where the speed of light has been normalized to 1, both s and t have units of mass squared, so we can plot them on the horizontal axis of Figure 3.1. Now, the Veneziano amplitude has a pole whenever $\alpha(t) = J$, for $J = 0, 1, 2, 3, \ldots$. This is equivalent to the poles occurring when $t = m^2_{\pi^i}$, since the Regge trajectory function gives us $\alpha(m^2_{\pi^i}) = J$, where J here represents integer values of spin.

Let us now investigate the behaviour of the function near the poles. At the t-poles, $-a_0 - a't = -J$ for positive integers J. To examine the behavior close to the t-poles, we will calculate $\Gamma(-J+\epsilon)$ for small ϵ.

$$\Gamma(-J+\epsilon) \approx \frac{(-1)^J}{\epsilon \cdot J!}$$

Since we are examining the region where $-a_0 - a't = -J + \epsilon$, we can express ϵ as $\epsilon = J - a_0 - a't$. Therefore,

$$\Gamma(-J+\epsilon) \approx \frac{(-1)^J}{(J-a_0-a't)\cdot J!} \tag{3.13}$$

If we consider that $J = a_0 + a't = a_0 + a'(m^2_{\pi^i})$, where m_{π^i} is the mass of the exchanged pion with spin i, then we can rewrite the expression in Equation 3.13 as

$$\frac{(-1)^{J+1}/a'}{J!(t-m^2_{\pi^i})} \frac{\Gamma(-a_0-a's)}{\Gamma(-J-a's-a_0)}.$$

We see that this expression reproduces the same poles (at $t = m^2_{\pi^i}$) that would arise upon summing

the infinite series of Feynman amplitudes we encountered previously. In addition,

$$\frac{\Gamma(-a_0 - a's)}{\Gamma(-J - a's - a_0)} = P_J(s)$$

is a polynomial of order J in s, and in the high energy (large s) limit gives

$$\frac{\Gamma(-a_0 - a's)}{\Gamma(-J - a_0 - a's)} \propto s^J$$

This matches what we got from the first two Feynman amplitudes we calculated - recall that $|\mathcal{M}_{\pi^0}|^2$ had no s in its numerator, while $|\mathcal{M}_{\pi^1}|^2$ contained an s^2 in its numerator.

High energy behavior

As $s \to \infty$, we can use Stirling's approximation for the gamma function

$$\Gamma(x) \approx (2\pi)^{\frac{1}{2}} e^{-x} x^{x-\frac{1}{2}}$$

as $x \to \infty$. Applying this to the Veneziano amplitude along with the Regge limit conditions, we obtain

$$\mathcal{A} = \frac{\Gamma(-\alpha(t))\Gamma(-\alpha(s))}{\Gamma(-\alpha(t) - \alpha(s))} \qquad \to \qquad K_o \Gamma(-\alpha(t))(-a')^{\alpha(t)} s^{\alpha(t)} \tag{3.14}$$

3.3 Comparison to spin-0

We can obtain the Reggeized propagator by expanding the Veneziano amplitude for $J = \alpha(t)$ close to 0 (corresponding to the lowest order contibution, from the spin-0 pion) and comparing it to the Feynman amplitude for the spin-0 propagator we obtained in Equation 3.5. Upon performing the expansion, we have

$$\mathcal{A} \approx \frac{K_o}{(-\alpha(t))} = \frac{-K_o/a'}{(t - m_{\pi^0}^2)}$$

We see that the amplitude $\mathcal{A} = K_o \Gamma(-\alpha(t))(-a')^{\alpha(t)} s^{\alpha(t)}$ from Equation 3.14 reduces to $K_o/-\alpha(t)$ upon considering only the contribution of the spin-0 pion. Carrying out this line of thinking in reverse, we argue that by replacing $K_o/(-\alpha(t))$ with $K_o \Gamma(-\alpha(t))(-a')^{\alpha(t)} s^{\alpha(t)}$ in the contribution to the amplitude from the spin-0 pion, we recover the contribution of the whole family of pions at high energy. This amounts to making the substitution

$$\boxed{\frac{1}{t - m_{\pi^0}^2} \to -a' \Gamma(-\alpha(t))(-a')^{\alpha(t)} s^{\alpha(t)}} \tag{3.15}$$

The expression $-a'\Gamma(-\alpha(t))(-a')^{\alpha(t)} s^{\alpha(t)}$ is what we call the Reggeized propagator. We can substitute this expression in the place of $\frac{1}{t - m_{\pi^0}^2}$ wherever it appears in any spin-0 propagator Feynman amplitudes

to recover the contribution of the entire family of pions.

3.4 Reggeized amplitude

In the previous section, we obtained an expression for the 'Reggeized' version of the pion propagator. What this means is that we can replace the spin-0 pion propagator factor in the calculation of the 2-3 scattering Feynman diagram in Figure 3.9 with the Reggeized propagator to obtain the amplitude containing the contribution of the entire Regge trajectory.

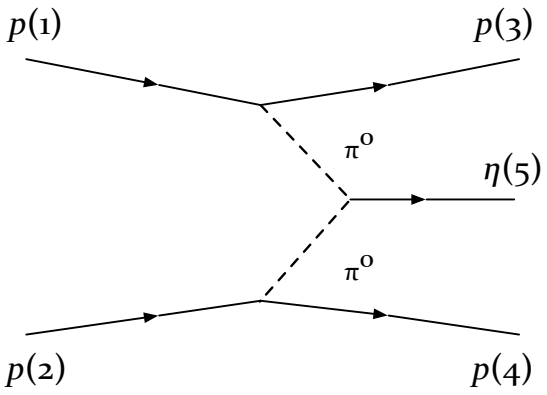

Figure 3.9: Feynman diagram representing 2-3 scattering via spin-0 pion exchange.

The Feynman amplitude for the 2-3 process mediated by spin-0 pion exchange is given by

$$\mathcal{M} = \int [\bar{u}_3(-ig_0)u_1]\frac{1}{q_1^2 - m_{\pi_0}^2}[-ig_1]\frac{1}{q_2^2 - m_{\pi_0}^2}[\bar{u}_4(-ig_0)u_2]$$
$$\times (2\pi)^4\delta^4(p_1 - q_1 - p_3)(2\pi)^4\delta^4(q_1 + q_2 - p_5)(2\pi)^4\delta^4(p_2 - q_2 - p_4)\frac{d^4q_1}{(2\pi)^4}\frac{d^4q_2}{(2\pi)^4}$$

Integrating over d^4q_1 and d^4q_2 using the delta function integral and simplifying, we have:

$$[\bar{u}_3(ig_0)u_1]\frac{1}{(p_1 - p_3)^2 - m_{\pi^0}^2}[-ig_1]\frac{1}{(p_2 - p_4)^2 - m_{\pi^0}^2}[\bar{u}_4(ig_0)u_2](2\pi)^4\delta^4(p_1 + p_2 - p_3 - p_4 - p_5)$$

Erasing the delta function, expressing the denominators in terms of our Mandelstam variables, and multiplying by i, we obtain the expression

$$\mathcal{M} = -g_0^2 g_1 \frac{[\bar{u}_3 u_1]}{(t_1^2 - m_{\pi^0}^2)}\frac{[\bar{u}_4 u_2]}{(t_2^2 - m_{\pi^0}^2)}$$

Again, we are interested in the average over the initial spins and sum over final spins, so we apply

Casimir's trick to the amplitude.

$$\langle|\mathcal{M}|^2\rangle = \frac{1}{4}\sum_{\text{all spins}} \frac{g_0^4 g_1^2}{(t_1^2 - m_{\pi^0}^2)^2 (t_2^2 - m_{\pi^0}^2)^2} [\bar{u}_3 u_1][\bar{u}_4 u_2][\bar{u}_3 u_1]^* [\bar{u}_4 u_2]^* \tag{3.16}$$

We have already calculated the expression

$$\sum_{\text{all spins}} [\bar{u}_3 u_1][\bar{u}_4 u_2][\bar{u}_3 u_1]^* [\bar{u}_4 u_2]^*$$

in Equation 3.4 to be $4(p_3 \cdot p_1 + m_p^2)(p_4 \cdot p_2 + m_p^2)$, which simplifies to $16(2m_p^2 + t_1/2)(2m_p^2 + t_2/2)$. Substituting this expression in Equation 3.16, we have

$$\langle|\mathcal{M}|^2\rangle = \frac{4 g_0^4 g_1^2}{(t_1 - m_{\pi^0}^2)^2 (t_2 - m_{\pi^0}^2)^2} \left(2m_p^2 - \frac{t_1}{2}\right)\left(2m_p^2 - \frac{t_2}{2}\right)$$

Taking the square root of the above, we obtain the spin-averaged magnitude of the scattering amplitude.

$$\langle|\mathcal{M}|\rangle = \frac{2 g_0^2 g_1}{(t_1 - m_{\pi^0}^2)(t_2 - m_{\pi^0}^2)} \sqrt{\left(2m_p^2 - \frac{t_1}{2}\right)\left(2m_p^2 - \frac{t_2}{2}\right)} \tag{3.17}$$

The above expression is the contribution of the spin-0 pion to the scattering amplitude. To include the contribution of the whole family of pions, we substitute the Reggeized propagator from Equation 3.15 for the spin-0 propagator in Equation 3.17. Our amplitude (dropping the spin-averaged notation) then becomes

$$\mathcal{M} = 2 g_0^2 g_1 [-a'\Gamma(-\alpha(t_1))(-a')^{\alpha(t_1)} s_1^{\alpha(t_1)}][-a'\Gamma(-\alpha(t_2))(-a')^{\alpha(t_2)} s_2^{\alpha(t_2)}] \sqrt{(2m_p^2 - t_1/2)(2m_p^2 - t_2/2)} \tag{3.18}$$

There is one last thing we will want to do before calculating $|\mathcal{M}|^2$ and the differential cross section. The pions that lie on the Regge trajectory (Figure 3.1) have even spin and contribute the most to the scattering amplitude. Our model should reflect this fact. To do this, we will introduce a modulating factor that eliminates the poles in the scattering amplitude due to odd-spin pion exchange. For 2-2 scattering, this factor is

$$\boxed{\mathcal{R} = \frac{1 + e^{i\pi\alpha(t)}}{2}}$$

At even values of $\alpha(t) = J$, $\mathcal{R}$ equals 1, and at odd values it goes to zero. Since the differential cross section is proportional to $|\mathcal{M}|^2$, the introduction of $\mathcal{R}$ in the scattering amplitude results in a factor of $|\mathcal{R}|^2$ in the differential cross-section (see Figure 3.10). In 2-3 scattering, we have two factors,

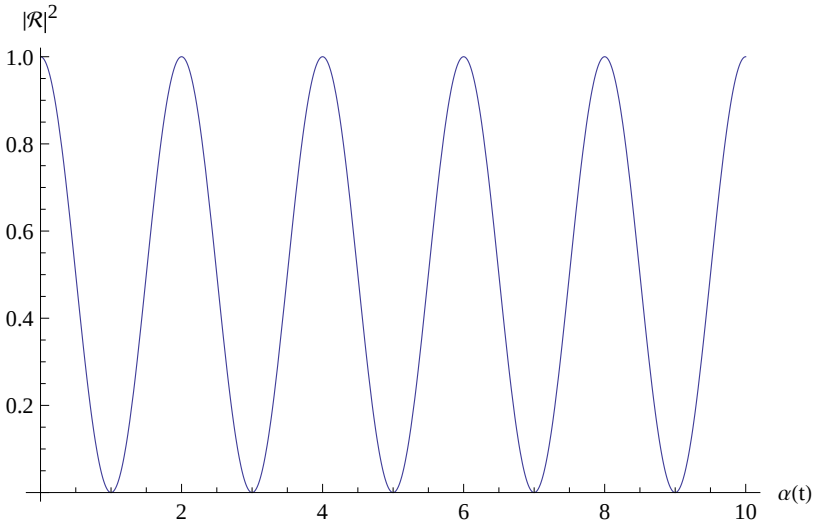

Figure 3.10: A plot of $|\mathcal{R}|^2$ vs. $\alpha(t)$. We can see how the modulating factor $\mathcal{R}$ suppresses the contributions of odd-spin pions while retaining the contribution of the pions with even spin - the function has peaks at even integer values of $\alpha(t)$ but drops to zero at odd integer values of $\alpha(t)$

corresponding to t_1 and t_2.

$$\boxed{\mathcal{R}_1 = \frac{1 + e^{i\pi\alpha(t_1)}}{2}} \qquad \boxed{\mathcal{R}_2 = \frac{1 + e^{i\pi\alpha(t_2)}}{2}}$$

To ensure the suppression of the odd-spin pions in the 2-3 scattering amplitude, we simply multiply $\mathcal{M}$ by both terms.

3.5 From the amplitude to the differential cross-section

Finally, we will want to express this amplitude in terms of the experimentally measured parameters. It's almost there, but we need to rewrite s_1 and s_2 in terms of t_1, t_2, x_F and θ_{34}. At this point, we will introduce slightly modified notation to be consistent with the literature.

$$p_{3z} = x_1 p, \qquad p_{4z} = -x_2 p \qquad \Rightarrow \qquad x_F = x_2 - x_1 \tag{3.19}$$

From the definition of s_1 and the mass-shell condition for particle 4, we obtain the relation

$$s_1 = s - 2\sqrt{s}E_4 + m_p^2 \tag{3.20}$$

We can manipulate the mass-shell condition for particle 4 to get

$$2\sqrt{s}E_4 = x_2 s \left(1 + \frac{4m_p^2(1 - x_2^2) - 4t_2)}{s x_2^2}\right)^{\frac{1}{2}}$$

Since the second term under the square root is extremely small (for very large values of s), we can perform a binomial expansion and keep only the leading order term. Substituting this expression for $2\sqrt{s}E_4$ in Equation 3.20, we get

$$s_1 = (1-x_2)s + m_p^2 + \frac{2t_2}{x_2} - \frac{2m_p^2(1-x_2^2)}{x_2}$$

In the right hand side of the above equation, all terms except for the first are negligible in the Regge limit. This implies that $s_1 \approx (1-x_2)s$. But we also know that $s >> s_1$. Therefore, $(1-x_2)$ must be extremely small to compensate for the large value of s. Similarly, we find that the terms $(1-x_1)$ is small. This implies that $p_{3z} \approx p$ and $p_{4z} \approx -p$, which is consistent with the Regge limit where the scattered protons are only slightly deflected from their original path. After these approximations, we get

$$s_1 = \left(1 - \frac{x_1+x_2}{2}\right)s - \frac{sx_F}{2} + m_p^2 + 2t_2 \tag{3.21}$$

Performing a similar process for s_2, we get

$$s_2 = s\left(1 - \frac{x_1+x_2}{2}\right) + \frac{sx_F}{2} + m_p^2 + 2t_1 \tag{3.22}$$

If we define the term $\eta = m_\eta^2 - t_1 - t_2 + \sqrt{t_1 t_2}\cos\theta_{34}$, we get the following relation from the mass shell condition for the η meson.

$$\sqrt{s}E_5 = \frac{s|x_F|}{2}\left(1 - \frac{4m_p^2}{s} + \frac{4\eta}{sx_F^2}\right)^{\frac{1}{2}} \approx \frac{s|x_F|}{2}\left(1 - \frac{2m_p^2}{s} + \frac{2\eta}{sx_F^2}\right)$$

By conservation of energy, we can get another expression for E_5:

$$E_5 = \frac{s_1 + s_2 - 2m_p^2}{2\sqrt{s}}$$

Substituting the values of s_1 and s_2 from Equation 3.21 and Equation 3.22 into the above expression, we obtain

$$\sqrt{s}E_5 = s\left(1 - \frac{x_1+x_2}{2}\right) + m_p^2 + (t_1+t_2)$$

Equating the two expressions for E_5 from conservation of energy and the mass-shell condition, we get the an expression for the first term on the right hand sides of Equation 3.20 and Equation 3.22 in terms of x_F, t_1, t_2 and η. We then substitute this expression back into our equations for s_1 and s_2 from Equation 3.21 and Equation 3.22 and get

$$\boxed{s_1 = |x_F|m_p^2 - (t_1-t_2) + \frac{\eta}{|x_F|} + \frac{s(|x_F|-x_F)}{2}} \quad \text{and} \quad \boxed{s_2 = |x_F|m_p^2 + (t_1-t_2) + \frac{\eta}{|x_F|} + \frac{s(|x_F|+x_F)}{2}}$$

Thus, for $x_F \geq 0$,

$$s_1 = m_p^2 x_F - (t_1 - t_2) + \frac{\eta}{x_F}$$

and

$$s_2 = m_p^2 x_F + (t_1 - t_2) + \frac{\eta}{x_F} + s x_F \approx s x_F$$

keeping only terms of order s in the Regge limit. For $x_F \leq 0$,

$$s_1 = - m_p^2 x_F - (t_1 - t_2) - \frac{\eta}{x_F} - s x_F \approx -s x_F$$

and

$$s_2 = -x_F m_p^2 + (t_1 - t_2) - \frac{\eta}{x_F}$$

Substituting the values of s_1 and s_2 (with the appropriate signs for x_F) back into the amplitude, we get the final form of $|\mathcal{M}|^2$.

$$\begin{aligned} |\mathcal{M}|^2 =& |\mathcal{R}_1|^2 |\mathcal{R}_2|^2 4 g_o^4 g_1^2 \left[\Gamma(-\alpha(t_1))(-\alpha')^{\alpha(t_1)+1} \left(m_p^2 x_F - (t_1 - t_2) + \frac{\eta}{x_F} \right)^{\alpha(t_1)} \right]^2 \\ & \times \left[\Gamma(-\alpha(t_2))(-\alpha')^{\alpha(t_2)+1} \left(s x_F \right)^{\alpha(t_2)} \right]^2 \\ & \times \left(2m_p^2 - \frac{t_1}{2} \right) \left(2m_p^2 - \frac{t_2}{2} \right) \qquad \text{for } x_F \geq 0 \end{aligned}$$

$$\begin{aligned} |\mathcal{M}|^2 =& |\mathcal{R}_1|^2 |\mathcal{R}_2|^2 4 g_o^4 g_1^2 \left[\Gamma(-\alpha(t_1))(-\alpha')^{\alpha(t_1)+1} \left(-s x_F \right)^{\alpha(t_1)} \right]^2 \\ & \times \left[\Gamma(-\alpha(t_2))(-\alpha')^{\alpha(t_2)+1} \left(-m_p^2 x_F + (t_1 - t_2) - \frac{\eta}{x_F} \right)^{\alpha(t_2)} \right]^2 \\ & \times \left(2m_p^2 - \frac{t_1}{2} \right) \left(2m_p^2 - \frac{t_2}{2} \right) \qquad \text{for } x_F \leq 0 \end{aligned}$$

This is the form of the amplitude that we will insert into our differential cross-section, that is, the probability distribution function that we will use to simulate the experiment. We expect to see exponential suppression as t_1 and t_2 become more negative. We also expect to see spikes in the number of scattering events as x_F goes to ± 1 or 0, because of the term $(1 - |x_F|)(|x_F|)$ in the denominator of the differential cross section. Finally, we expect a weak dependence on θ_{34}, since it is buried in the term η and has a relatively small contribution compared to the other parameters.

Chapter 4

Simulation

In this chapter we will use numerical methods to simulate large numbers of scattering events using the differential cross-section we have calculated. In the preceding chapters, we established that the total scattering cross-section σ for the process $p + p \rightarrow p + p + \eta$ is given by the expression

$$\sigma = \int \left(\frac{|\mathcal{M}|^2}{4096\pi^4 s^2 \sqrt{s}(1 - |x_F|)(|x_F|)} \right) dt_1 dt_2 dx_F d\theta_{34} \tag{4.1}$$

However, as you may have guessed from seeing the form of $|\mathcal{M}_{\text{mod}}|^2$ from chapter 3, this integral is not analytically tractable. Besides, the quantity that experimentalists measure is often not the total cross-section but the differential cross-section with respect to one of t_1, t_2, x_F and θ_{34}. By generating events numerically, we can simulate the distribution of the frequency of scattering events with respect to all four of these parameters and compare it with experimental data.

As explained earlier, σ is an integral over all possible values of t_1, t_2, x_F and θ_{34}. In the absence of the term in the large brackets, the differential cross-section, all combinations of values of these variables would be equally probable. However, the presence of the term modulates the probability distribution, so that certain values are 'favored' more often than others. Thus, to simulate the experiment, we need to generate random combinations of outgoing momenta (in practice, combinations of t_1, t_2, x_F and θ_{34}) consistent with the probability distribution function given by $|\mathcal{M}|^2$. In the language of particle physics, these combinations are known as *events* and our primary task in this act of the thesis is to build a *event generator* - a program to output random numbers corresponding to particle scattering events.

4.1 Random numbers

Generating random numbers according to a given probability distribution is an interesting exercise in itself. We will be generating what are essentially random coordinates in a 4-dimensional space. Since the number of dimensions is relatively low, we can use a simple yet powerful method known as the *rejection method*.

Rejection method in one dimension

We will start with generating random numbers in one dimension according to a given probability distribution, and work our way up from there. Consider the probability distribution function (p.d.f.):

$$\rho(x) = \frac{1}{\sqrt{\pi}} e^{-x^2} \tag{4.2}$$

Observe its plot below:

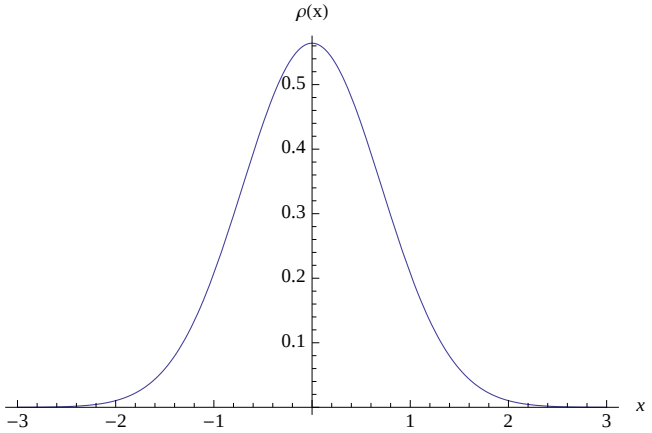

Figure 4.1: Plot of the probability distribution function $\rho(x) = \frac{1}{\sqrt{\pi}} e^{-x^2}$

Roughly speaking, if we generate random numbers according to this distribution, they will be generated more frequently in regions where $\rho(x)$ is high. This means that, for example, there will be a greater concentration of random numbers between 0 and 1 than there will be between 1 and 2, since the value of $\rho(x)$ is lower in that region. As a corollary, if we construct a histogram of the random numbers, the peaks of the bars should roughly correspond to the shape of the distribution. Consider a box that surrounds the plot above. Obviously, it does not surround the whole curve, but we see that the probability of a random number being generated outside $x \in (-3, 3)$ is close to zero, so we will only consider this region. The upper and lower edges of the box are at the maximum and minimum of the function $\rho(x)$ on the interval $x \in (-3, 3)$, and the left and right edges are at $x = -3$ and $x = 3$, respectively. The rejection method follows the algorithm below:

1. Generate a set of random points, uniformly distributed in the interior of the bounding box.[1] These will be ordered pairs.

2. If a point lies within the area under the probability distribution curve, we accept the x-coordinate of the ordered pair into our final set of random numbers, otherwise we reject it. A simple test to see whether the point (x, y) lies within the area is to see if $y \leq \rho(x)$. If yes, then it does lie within the area under the curve, and x is an acceptable random number.

[1]The generation of uniform random numbers (also known as uniform deviates) is a whole subfield of numerical methods in itself - here we will just use *Mathematica*'s inbuilt **`RandomReal`** function to generate uniform deviates within a certain region. Our main focus will be on generating 'modified' deviates according to a given p.d.f. from uniform deviates.

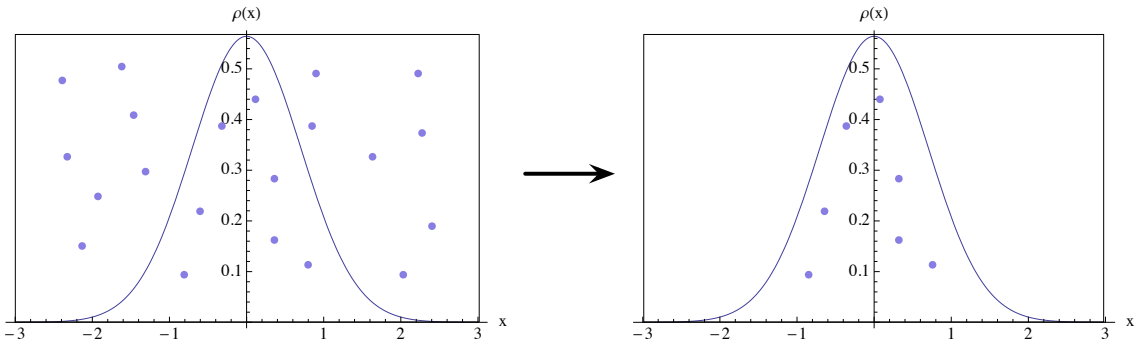

Figure 4.2: An illustration of the acceptance-rejection method for the one-dimensional probability distribution function shown in Figure 4.1. Random points are generated in the bounding box of the function, uniformly distributed on its interior. Out of these, the ones that lie below the curve are accepted and the the rest are rejected. The list of x values that we get from the accepted points is a list of random numbers that follow the given probability distribution function.

It should be clear that this method will produce exactly the distribution of random numbers we want - there will be more points under regions of the curve with higher values of $\rho(x)$, leading to more acceptable random numbers in that x-region. Figure 4.3 shows a histogram with bin width 0.1, generated with *Mathematica*'s inbuilt **`Histogram`** command. As you can see, the profile of the histogram clearly matches the shape of the p.d.f.!

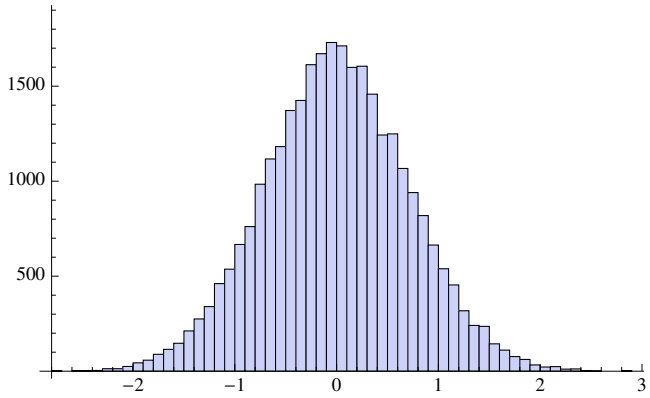

Figure 4.3: 100,000 random points (events) were generated on the range $x \in [-3, 3]$ and $y \in [0, 1]^3$ according to the probability distribution function in Equation 4.2, and 29,507 of them were found acceptable. This is a histogram showing their distribution with respect to x.

Of course, the tighter the bounding shape fits the p.d.f. curve, the more efficient this method becomes, as fewer points are 'wasted' and we will not need to generate quite so many points to reasonably comply with the probability distribution. However, the shape of the p.d.f. in four dimensions is not well known, so it is best to stick with the rectangular bounding box. This method can be generalized to as many dimensions as we want, as long as we are willing to sample a large number of points.

Two dimensions

Let us now examine the problem of generating random numbers according to a probability distribution function in two dimensions. Consider the slightly more involved 2-dimensional p.d.f.

$$\rho(x, y) = 2 \sin^2 x \sin^2 y$$

shown in Figure 4.4. The procedure for generating random numbers according to a two-dimensional

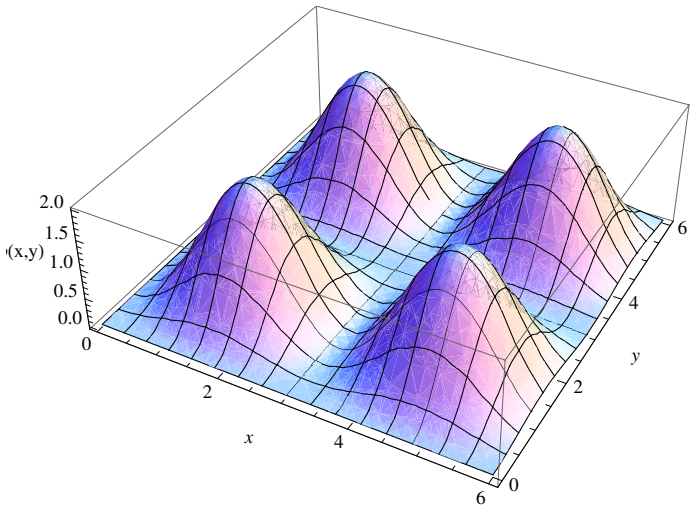

Figure 4.4: Plot of the probability distribution function $\rho(x, y) = 2 \sin^2 x \sin^2 y$ on the domain $x \in [0, 6]$, $y \in [0, 6]$

p.d.f. is almost exactly the same as in the one-dimensional case. Instead of a two-dimensional bounding box, we will consider a three-dimensional bounding cuboid that envelopes the plot and generate points uniformly within its interior. We will then accept the points that lie below the 2-D surface $\rho(x, y)$ and reject the points that lie above it. Our test for this is to examine each point $\{x, y, z\}$ to see whether $z \leq \rho(x, y)$. If so, then $\{x, y\}$ is an acceptable combination, or event. Following a similar procedure, we can generalize this method to pick out points lying under a 4-D curve embedded in 5-D space.[4]

Four dimensions

The points that we will generate will be ordered pairs of the form $\{t_1, t_2, x_F, \theta_{34}, k\}$. 8 of the 'edges' of the bounding box in 5 dimensions will correspond to physically inspired upper and lower limits for each of the four variables, and the remaining two will be determined by the maximum and minimum value that the p.d.f. (in this case, the differential cross-section) takes on the specified domain.

[4]One limitation that should be pointed out is that this method gets less efficient with each extra dimension - obviously, more points are needed to uniformly fill a 3-D cube than a 2-D square with the same edge length, and the same idea applies to higher dimensions.

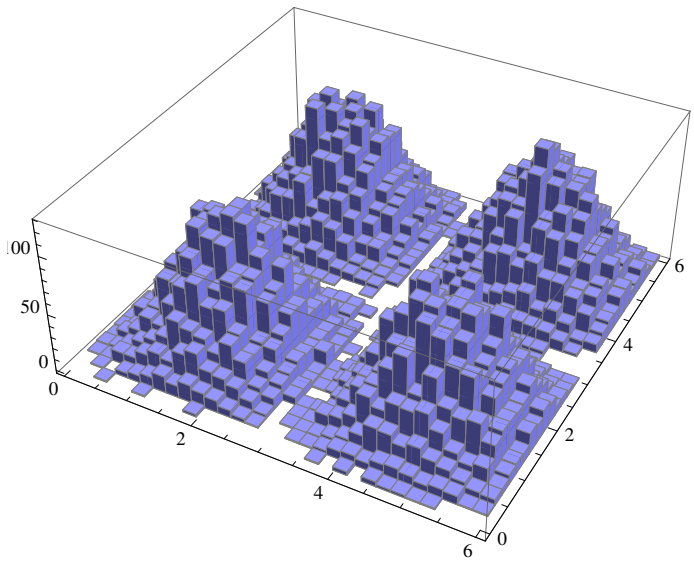

Figure 4.5: Histogram showing the distribution of 27,135 random events modulated by the 2-D p.d.f. $\rho(x,y) = 2\sin^2 x \sin^2 y$, on the domain $x \in [0,6]$, $y \in [0,6]$. Note how the profile of the histogram corresponds to the shape of the p.d.f. curve in Figure 4.4.

4.2 Event generation

Limits

In this section we will discuss the 'physically inspired limits' mentioned earlier. This will help us define our five-dimensional bounding box.

Limits of x_F

Recall that x_F is defined by

$$x_F = x_2 - x_1$$

In the small angle scattering limit, we have seen that $x_2 \approx 1$ and $x_1 \approx 1$. In a sense, x_1 and x_2 simply tell us the extent of the deflection of the two incoming protons. This can range from 'not deflected at all' ($x_1, x_2 = 1$) to 'scattered at a right angle, with only components in the x and y directions. ' ($x_1, x_2 = 0$). Applying these extreme limits, we end up with the overall limit for x_F:

$$-1 \leq x_F \leq 1$$

Limits of t_1 and t_2

We consider both t_1 and t_2 to range from 0 to -0.6 GeV^2. We believe that below this threshold, perturbative QCD effects kick in and our model stops working. Additionally, when we perform the simulation, it turns out that due to exponential suppression of $|\mathcal{M}|^2$ in t_1 and t_2, the probability of an event occurring outside this zero is nearly zero.

Limits of θ_{34}

Taking all possible non-redundant values, θ_{34} ranges from 0 to π.

Regge trajectory

The Regge trajectory function was found by fitting a linear function to the π^0, π^2, and π^4 mesons on the Chew-Frautschi plot. Performing a least-squares fit to the data using *Mathematica*'s inbuilt **`Fit`** function, we get the Regge trajectory function as

$$\alpha(x) = -0.0734355 + 0.79042x$$

The unit of mass and energy used in this simulation is GeV (giga electron volts).

Parameters

The coupling constants g_0 and g_1 were normalized to 1 each, reflecting the high strength of the interaction. In any case, this will not affect the distribution of the events in any of the four parameters, since they were essentially just constant scaling factors. The mass of the proton was taken to be 0.938 GeV, and the mass of the η meson was input as 0.548 GeV. $\sqrt{s}$, the CM energy, is taken to be 7 TeV (tera electron volts), which corresponds to the energies at the Large Hadron Collider.

4.3 Results

Using our event generator, we generated 69,188 events corresponding to the differential cross-section p.d.f. The distribution of the events is shown in the histograms in Figure 4.6. The horizontal axis corresponds to the parameter and the vertical axis denotes the number of scattering events. We see that the simulation reproduces the expected behavior based on the form of the scattering amplitude: the exponential suppression in t_1 and t_2 as they go to -0.6 GeV^2, an increased number of scattering events near $x_F = \pm 1$ and $x_F = 0$ and a weak dependence on θ_{34}. This simulation can be used to compare our model to experimental data from the LHC and other particle colliders.

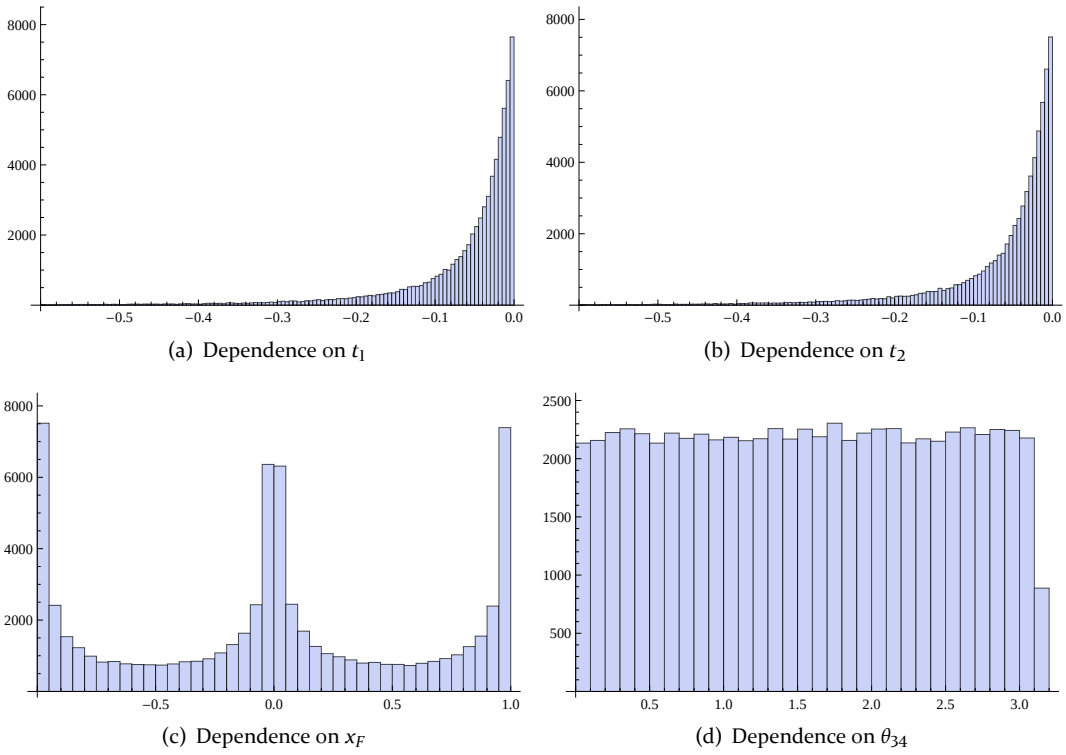

(a) Dependence on t_1

(b) Dependence on t_2

(c) Dependence on x_F

(d) Dependence on θ_{34}

Figure 4.6: Distribution of 69,188 scattering events in t_1, t_2, x_F and θ_{34} at $\sqrt{s}$ = 7 TeV. The distributions are qualitatively consistent with our model. The dip in θ_{34} near $\theta_{34} = \pi$ is an artifact of the histogram generation method, since the final histogram bin includes values of $\theta_{34} \geq \pi$, outside our simulation limit.

Conclusion

In this thesis we developed a model for proton/proton scattering in the Regge limit of high energy and small angular deflection. This model postulates that the interaction between the protons is mediated by a family of neutral pions with increasing spins, known as a 'Regge trajectory'. At low energies, it is sufficient to consider the contribution of just the lowest-spin member of the family to the interaction, but at high energies we must consider the contribution of the whole family. We first set up the relativistic kinematics of the process using Lorentz-invariant Mandelstam variables, and performed approximations consistent with the Regge limit. The next step was to find the meeting place between theory and experiment - we obtained the form of the differential cross-section that depended on the actual parameters that experimentalists measure. We then introduced the Veneziano amplitude as an expression for 2-2 proton/proton scattering via the exchange of neutral pion Regge trajectories, and motivated it by showing how it reproduced the pole structure and s-dependence that we found in the corresponding series of Feynman amplitudes. We expanded the high energy form of the Veneziano amplitude near spin 0 to find the 'Reggeized propagator'. This propagator, when substituted in the Feynman amplitude of the 2-3 scattering process $p + p \rightarrow p + p + \eta$ occurring via the exchange of spin-0 pions gives us the amplitude from the exchange of the entire Regge trajectory. Inserting this amplitude into the form of the differential cross-section obtained earlier gave us a concrete probability distribution function that we could use to simulate the experiment. An event generator was implemented in *Mathematica* to simulate scattering events. The distribution of scattering events with respect to the various parameters obtained from the simulation reproduced the qualitative behavior we expected to see based on the form of the scattering amplitude. Suggestions for further work include comparing the simulated distribution of scattering events based on this model with actual scattering data from high energy particle accelerators such as the LHC.

This thesis has not strayed very far from the realm of experiment at any point. Indeed, every stage of development of the model keeps experimental considerations in mind. To conclude, this proximity to experiment is a healthy one for us theorists to aspire to, even if it cannot always be maintained. Also, I cannot resist adding that the experimental verification of this model would be a metaphorical brick in the foundation of string theory, corroborating it at least a little and increasing its chances of proving to be a framework that incorporates the standard model and physics beyond it.

Appendix A

Mathematica Code

This appendix contains the *Mathematica* code I used to simulate the experiment. The *Mathematica* notebook that contains this and the code for the 1-D and 2-D p.d.f.s can be downloaded at **www.adarshpyarelal.com/research/reedthesis**.

```
Randoms4D[function_, t1limits_, t2limits_, xFlimits_, θ34limits_, num_] :=
 Module[{uniformtab, randomstab, rejectionstab, boxlimits},
  boxlimits =
   {MinValue[{function[t1, t2, xF, θ34], t1limits[[1]] ≤ t1 ≤ t1limits[[2]],
      t2limits[[1]] ≤ t2 ≤ t2limits[[2]], xFlimits[[1]] ≤ xF ≤ xFlimits[[2]],
      θ34limits[[1]] ≤ θ34 ≤ θ34limits[[2]]}, {t1, t2, xF, θ34}],
    MaxValue[{function[t1, t2, xF, θ34], t1limits[[1]] ≤ t1 ≤ t1limits[[2]],
      t2limits[[1]] ≤ t2 ≤ t2limits[[2]], xFlimits[[1]] ≤ xF ≤ xFlimits[[2]],
      θ34limits[[1]] ≤ θ34 ≤ θ34limits[[2]]}, {t1, t2, xF, θ34}]};
  uniformtab =
   Table[{RandomReal[{t1limits[[1]], t1limits[[2]]}],
     RandomReal[{t2limits[[1]], t2limits[[2]]}],
     RandomReal[{xFlimits[[1]], xFlimits[[2]]}],
     RandomReal[{θ34limits[[1]], θ34limits[[2]]}],
     RandomReal[{boxlimits[[1]], boxlimits[[2]]}]}, {i, 1, num}];
  rejectionstab =
   Table[
    If[uniformtab[[i, 5]] < function[uniformtab[[i, 1]], uniformtab[[i, 2]],
       uniformtab[[i, 3]], uniformtab[[i, 4]]],
     {uniformtab[[i, 1]], uniformtab[[i, 2]], uniformtab[[i, 3]],
      uniformtab[[i, 4]]}, 0.], {i, 1, Length[uniformtab]}];
  randomstab = Select[rejectionstab, # ≠ {0.} &];
  Return[randomstab];
 ]
```

Figure A.1: The function **Randoms4D** generates combinations of random numbers given a four-dimensional probability distribution function $\rho(t_1, t_2, x_F, \theta_{34})$, and the limits of each of the four variables.

```
Histograms4D[randomstab_] := Module[{tab, t1hist, t2hist, xFhist, θ34hist},
  tab = randomstab;
  t1hist = Histogram[Table[tab[[i, 1]], {i, 1, Length[tab]}], PlotRange → All];
  t2hist = Histogram[Table[tab[[i, 2]], {i, 1, Length[tab]}], PlotRange → All];
  xFhist = Histogram[Table[tab[[i, 3]], {i, 1, Length[tab]}], PlotRange → All];
  θ34hist = Histogram[Table[tab[[i, 4]], {i, 1, Length[tab]}], PlotRange → All];
  Return[{t1hist, t2hist, xFhist, θ34hist}];
 ]
```

Figure A.2: The function **Histograms4D** creates histograms showing the dependence of the frequency of scattering events upon the four variables t_1, t_2, x_F and θ_{34}.

Bibliography

[1] F. Balestra *et al.*, *Exclusive eta production in proton-proton reactions,* Phys. Rev. C **69**, 064003 (2004).

[2] D.C. Cheng and G.K. O'Neill, *Elementary particle physics: An Introduction*. Addison-Wesley, January 1979.

[3] P. D. B. Collins, *An Introduction to Regge Theory and High Energy Physics*. Cambridge University Press, 2009.

[4] S. K. Domokos, J. A. Harvey and N. Mann, *The Pomeron contribution to p p and p anti-p scattering in AdS/QCD,* Phys. Rev. D **80**, 126015 (2009).

[5] B. Greene, *The Elegant Universe: Superstrings, Hidden Dimensions, and the Quest for the Ultimate Theory*. W. W. Norton & Company, 1230.

[6] D. Griffiths, *Introduction to Elementary Particles*. Wiley-VCH, 2008.

[7] C. M. G. Lattes, H. Muirhead, G. P. S. Occhialini, and C. F. Powell. *Processes involving charged mesons*. *Nature*, 159(4047):694--697, May 1947.

[8] S. Mandelstam, *Determination of the Pion-Nucleon Scattering Amplitude from Dispersion Relations and Unitarity. General Theory*. *Physical Review*, 112(4):1344--1360, November 1958.

[9] O. Nachtmann, *Elementary particle physics: concepts and phenomena*. Springer-Verlag, 1990.

[10] K. Nakamura, Review of Particle Physics. *Journal of Physics G: Nuclear and Particle Physics*, 37(7A):075021, July 2010.

[11] J. G. Polchinski, *String theory: An introduction to the bosonic string, Volume 1*. Cambridge University Press, 1998.

[12] T. Regge, *Introduction to complex orbital momenta*. Il Nuovo Cimento, 14(5):951--976, December 1959.

[13] G. Veneziano, *Construction of a crossing-symmetric, Regge-behaved amplitude for linearly rising trajectories*. Il Nuovo Cimento A, 57(1):190--197, September 1968.

[14] B. Zwiebach, *A First Course in String Theory*. Cambridge University Press, 2004.